Assessing Storm Surge Impacts on Coastal Inundation due to Climate Change: Case Studies of Baltimore and Dorchester County in Maryland

Authors: Ming Li[1*], Fan Zhang[1], Samuel Barnes[2], and Xiaohong Wang[2]

Affiliation:

[1]Horn Point Lab, University of Maryland Center for Environmental Science, Cambridge, Maryland 21613, U.S.A.

[2]Department of Mathematics and Computer Science, Salisbury University, 1101 Camden Avenue, Salisbury, Maryland 21801, U.S.A.

ORCID: Ming Li (0000-0003-1492-4127), Fan Zhang (0000-0002-9637-0529).

Acknowledgments:

We are grateful to two reviewers for the helpful comments. Funding support was provided by Maryland Sea Grant (NA14OAR4170090 and SA75281450-H). Fan Zhang is supported by Maryland Sea Grant Fellowship. This is UMCES contribution number xxxx.

Submitted to *Natural Hazards*

*Correspondence to: Ming Li, Horn Point Lab, University of Maryland Center for Environmental Science, Cambridge, Maryland 21613, U.S.A. Email: mingli@umces.edu.

Abstract

Hurricane Isabel (2003) generated record flooding around Chesapeake Bay and caused extensive damage in rural Eastern Shore of Maryland and metropolitan cities like Baltimore. Regional atmosphere-ocean models are used to investigate the storm surge and coastal inundation that might be produced by a similar storm under the warmer ocean temperature and higher sea level projected for the future climate. Warming causes the storm to intensify, with the minimum sea level pressure decreasing from 955 mb during Isabel to ~950 mb in 2050 and ~940 mb in 2100. The stronger storm and higher mean sea level amplify the peak water level by ~0.5 m in 2050 and ~1.2 m in 2100. The total inundated area over Chesapeake Bay expands by 26% in 2050 and 47-62% in 2100. Over the rural Dorchester County, the inundated area shows moderate expansion in the future climate but the average inundation depth is 30% higher in 2050 and 50-70% higher in 2100. The number of houses flooded increases from 1,420 during Hurricane Isabel to 1,850/2,190 in 2100 under the climate change scenario Representative Concentration Pathway (RCP) 4.5/8.5. The inundated area in Baltimore is 2.2 km^2 during Hurricane Isabel, expands to 5.1 km^2 in 2050, and reaches 8.1/9.1 km^2 in 2100 under RCP 4.5/8.5. The estimated flood damage to Baltimore increases from $29 million in 2003 to $98/100 million in 2050 and $150/162 million in 2100 under the median projection of RCP 4.5/8.5. These estimates are subjected to uncertainty due to different climate change scenarios and different climate model projections.

Keywords: coastal inundation, climate change, sea level rise, storm surge, economic loss, impact assessment.

1. Introduction

As demonstrated during recent catastrophic events such as Hurricane Sandy (2012), Hurricane Harvey (2017) and Hurricane Irma (2017), coastal communities, properties, and natural resources are at great risk to coastal inundation caused by storm surge. Since the 19th century, storm surge has cost millions of lives and hundreds of billions dollars in economic damage (El-Sabh 1990; USGCRP 2017). Climate change is expected to increase the rate of sea-level rise (IPCC 2013; Church et al. 2013) and cause significant increases in extreme weather (Emanuel et al. 2008; Wollings et al. 2012; Knutson et al. 2013; Eichler et al. 2013), exacerbating the coastal inundation problem. There is thus an urgent need to assess the potential impacts of storms on coastal inundation in the future climate.

Sea level rise leads to higher extreme sea levels and more extensive coastal flooding (Hallegatte et al. 2013; Hinkel et el. 2014; Sweet and Park 2014; Moftakhari et al. 2015). Tide gauge records and satellite altimetry reveal that global-mean sea level (GSML) rose at a rate of 1.2 ± 0.2 mm yr^{-1} between 1900 and 1990 and at a much faster rate of 3.0 ± 0.7 mm yr^{-1} between 1993 and 2012 (Domingues et al. 2008; Church and White 2011; Hay et al. 2015; Dangendorf et al. 2017). Climate models predict that the rate of sea level rise will accelerate in the 21st century. According to IPCC AR5 (Fifth Assessment Report of the Intergovernmental Panel on Climate Change), GMSL is projected to rise 0.52-0.98 m by 2100 for the highest emission scenario considered – Representative Concentration Pathway (RCP) 8.5 (Church et al. 2013). Probabilistic sea level projections suggest a very likely (90% probability) GMSL rise of 0.5-1.2 m under RCP 8.5 (Kopp et al. 2014). If the rapid collapse of Antarctic ice sheet as projected in some climate models is taken into consideration, the median projected GMSL for 2100 will increase from 0.79 to 1.46 m under RCP 8.5 (Kopp et al. 2017).

71 Some parts of the ocean rise faster than others. For example, tide-gauge records in
72 Chesapeake Bay show that sea levels increased by 3-4 mm per year over the 20th century (Zervas
73 2001, 2009), twice that of the global average. Land subsidence associated with glacial isostatic
74 adjustment is a dominant contributor to the high relative sea level rise (Engelhart et al. 2009;
75 Miller et al. 2013). Ocean dynamics, arising from changing ocean circulation, may also
76 contribute to higher sea levels in certain coastal regions. Sallenger et al. (2012) presented
77 evidence that the US East Coast north of Cape Hatteras is a hot spot of sea level rise. The
78 weakening of the Gulf Stream over the past decade may have contributed to the higher rates of
79 sea level rise along the Mid-Atlantic coast (Ezer and Corlett 2012; Ezer 2013; Ezer et al. 2013;
80 Kopp 2013). The Atlantic Meridional Overturning Current (AMOC), of which the Gulf Stream is
81 an essential component, is predicted to weaken during the 21st century (Yin et al 2009, 2010; Yin
82 and Goddard 2013), further raising sea levels along the U.S. East Coast. However, recent
83 analysis showed that sea level declined north of Cape Hatteras between 2010 and 2015 and this
84 decline was caused by an increase in atmospheric pressure combined with shifting wind patterns
85 (Domingues et al. 2018). Pieuch et al. (2018) suggested that river discharge may be a driver of
86 regional sea level variability along U.S. East and Gulf coasts.

87 Will extreme weather events such as hurricanes become more frequent and more severe
88 in a warming climate? Studies based on coarse-resolution General Circulation Models (GCMs)
89 have generally agreed on a tendency toward decreasing frequency and increasing intensity of
90 tropical cyclones as the climate warms (Bengtsson et al. 1996). On the other hand, a consensus
91 of GCMs predicts increasing wind shear over the North Atlantic with warming (Vecchi and
92 Soden 2007), which would tend to inhibit overall tropical cyclone activity. Using an ensemble of
93 GCMs and scenarios from phases 3 and 5 of the Coupled Model Intercomparison Project

(CMIP3 and CMIP5), Knutson et al. (2013) conducted dynamic downscaling projections of the 21st-century Atlantic hurricane activity. They found a significant reduction in the overall tropical storm frequency but a significant increase in the frequency of intense storms. Similar results were found in statistical-dynamic models (Emanuel 2006, 2008; Lin et al. 2012). However, Emanuel (2013) found that tropical cyclones over most oceans are projected to increase not only in intensity but also in frequency during the 21st century under RCP 8.5. Extratropical winter storms are also likely to change in the future climate. There is a remarkable consensus among climate models that the overall frequency of such storms will decline while the frequency of severe storms will increase (Wollings et al. 2012).

The combination of stronger storms and sea level rise will likely result in higher water levels and more extensive inundation in the future climate. However, assessing the climate change impacts on coastal inundation faces many challenges. Chief among them are the large uncertainty in sea level rise projections in the second half of 21st century (Kopp et al. 2017), the inherent difficulty of global climate models in predicting future storms, long-term geomorphological changes in coastal regions (Bilskie et al. 2016), and coastline management decisions under the threat of climate change and sea level rise (Holleman and Stacey 2014; Lee et al. 2017; Zhang and Li 2019). Moreover, engineering projects such as navigation channel dredging have led to significant increases in tidal range and storm surge height in many estuaries, including the Cape Fear River estuary, North Carolina (Familkhalili and Talke 2016) and the Hudson River estuary (Ralston et al. 2019). Interestingly, however, the mean water level in the upper part of the Hudson River decreased as a result of channel deepening such that the overall flooding risk was reduced.

Several methods have been proposed to examine the coastal inundation risk under a changing climate: dynamic climate downscaling approach, statistical deterministic approach, and perturbed historical baseline approach (Mcinnes et al. 2003; Bilskie et al. 2016). In the dynamic downscaling approach, high resolution regional atmosphere models capable of simulating hurricanes and tropical storms are nested within the coarse-resolution GCMs under the future climate condition (Lowe and Gregory 2005; Knutson and Tuleya 2004; Woth et al. 2006; Mallard et al. 2013a, b; Knutson et al. 2013). This is the most direct approach for assessing the climatic impacts on storms but is computationally prohibitive and inherits biases in the GCMs. In the statistical deterministic model, synthetic storms are generated from a statistical deterministic hurricane model (Emanuel et al. 2006) under large-scale atmospheric and oceanic environments as projected by GCMs (Mousavi et al. 2011; Hagen and Bacopoulos 2012; Lin et al. 2012, 2016). Using these synthetic storms to drive a hydrodynamic model, Lin et al. (2012) showed that the combined effects of storm climatology change and 1 m sea level rise may cause the present New York City 100-year surge flooding to occur every 3-20 years by the end of 21st century. In the perturbed historical approach, the hydrodynamic model is forced with historical extreme sea levels to obtain a baseline, and changes to the mean seal level and hurricane intensity are included in the model simulations (Yang et al. 2014; Orton et al. 2015, 2018). A few studies use a hybrid of these approaches. For example, Mousavi et al. (2011) investigated three historical storms and used an empirical deterministic model to account for the changes in the storm intensity due to warming ocean.

Previous studies have suggested that the cumulative effects of sea level rise, tides and storm surges on coastal inundations are not simple linear additions. Smith et al. (2010) found that sea level rise can greatly amplify surge heights in shallow wetland areas of southeast Louisiana.

Surge generation and propagation over shallow areas are nonlinear processes and sensitive to changes in the water depth. There are also strong interactions between storm surges and tides (Horsburgh and Wilson 2007). Mikhailva (2011) examined sea level observations in the Elbe River, Germany, and found that mean sea level, tidal range, and storm surges all increased during the second half of the 20th century. When changes in storm climate is considered, Lin et al. (2016) found that Hurricane Sandy's flooding frequency at New York City significantly increases over 21st century compared to the scenario with sea level rise alone. Large-scale climate variabilities such as the North Atlantic Oscillation and geomorphic changes due to dredging or shoreline hardening may have also contributed to higher sea level extremes in recent decades (Talke et al. 2014; Marcos et al. 2015; Familkhalili and Talke 2016; Ralston et al. 2019).

Besides the physics of sea level rise, storm surge and extreme sea levels, a number of studies have investigated the socio-economic impacts of coastal flooding (e.g. Nicholls 2004; Hinkel et al. 2013; McNamara et al. 2015; Kulp and Strauss 2017; McAlphine and Porter 2018). For example, Hinkel et al. (2014) estimated that 0.2-4.6% of global population will be flooded annually in 2100 under 0.25-1.23 m GMSL rise, with expected annual loss of 0.3-9.3% of global domestic product. For the U.S., Hauer et al. (2016) projected that a 2100 sea level rise of 0.9 m will put 4.2 million people at the risk of coastal inundation. Neumann et al. (2015) examined the joint effects of storm surge and sea level rise in economic damage. Dinan (2017) suggested that the combined forces of climate change and coastal development will cause hurricane damage to increase faster than the U.S. economy is expected to grow in the 21st century. Other studies have analyzed how coastal mitigation and adaptation may alleviate the socio-economic impacts of coastal inundation (e.g. Neumann et al. 2011; Hallegatte et al. 2013). For example, Diaz (2016) used an optimization model to determine the optimal strategy for adaptation. McNamara et al.

(2015) developed a stochastic dynamic model coupling coastal property markets and shoreline evolution, and found that the policy-induced inflation of property value grows with increased erosion from sea level rise or increased storminess.

The coastal plains surrounding Chesapeake Bay feature many low-lying areas with low topographic relief (Wu et al. 2009), and are thus a good site for studying coastal inundation in a changing climate. Recurrent flooding at high tides is already a major problem (Mitchell et al. 2012) and will likely become more frequent in the future as sea level rises (Spanger-Siegfried et al. 2014). Chesapeake Bay is also susceptible to flooding by storm surges: about two dozens of hurricanes and tropical storms have moved past the Chesapeake Bay region over the past 20 years. In particular, Category 2 Hurricane Isabel made landfall over the Outer Banks of North Carolina on 18 September 2003 and moved northward on the west side of Chesapeake Bay, creating widespread flooding in Norfolk, Washington, D.C., Annapolis, Baltimore and rural Eastern Shore of Maryland and Virginia (Li et al. 2006, 2007; Shen et al. 2006; Zhong et al. 2010), as shown in Figure 1. This flooding event is considered to be a 100-year flooding event for planning purposes by cities and towns around Chesapeake Bay. A major open question is how much flooding such a storm may generate in 2050 or 2100 when the mean sea level and ocean temperature are higher. To address this, we use regional atmosphere-ocean models to simulate Hurricane Isabel (2003) and Isabel-like storms in the future climate as projected by the global climate models. Our approach goes beyond previous studies on storm surge because a regional atmosphere model is used to directly simulate the effects of ocean warming on hurricanes. Unlike the parametric surface wind model/planetary boundary wind model (Scheffner and Fitzpatrick 1997; Peng et al. 2004) and statistical-deterministic models (Lin et al. 2012, 2016), the regional atmosphere model can simulate the full hurricane dynamics including

185 mesoscale wind structures and wind speed asymmetry. An accurate wind field is critical for an
186 accurate prediction of storm surge along complex coastlines such as estuaries and bays (Chen et
187 al. 2013; Kerr et al. 2013). Coastal inundation maps obtained from the regional atmosphere-
188 ocean models will provide a more realistic depiction of coastal flooding over land during a storm
189 than those obtained from a storm surge model forced by the parametric winds of a hurricane
190 vortex.

191 We will investigate first the storm surge and coastal inundation over the entire estuary
192 and then provide detailed assessments on flooding and economic damage at two representative
193 sites. The City of Baltimore is chosen as a representative urban site, and the Dorchester County
194 on the Eastern Shore of Maryland is chosen as a representative rural area. By comparing the
195 responses of an urban and a rural site to the same storms, we can gain a better understanding of
196 their risks. Our goal is not to produce a probabilistic prediction for the storm surge and flooding
197 in the mid and late 21st century but rather to illustrate how ocean warming and sea level rise
198 affect the peak water level and coastal inundation in a coastal region. Although similar studies
199 were conducted on other coastal waters, storm surge response to hurricanes is highly dependent
200 on bathymetry and coastline geometry. The semi-enclosed nature of an estuary like Chesapeake
201 Bay can trap and amplify storm flooding, making it particularly vulnerable to coastal inundation.

202

203 **2. Methods**

204 To assess potential impacts of climate change on storm surge and coastal inundation, we
205 use regional atmosphere and ocean models. The regional atmosphere model, based on Weather
206 Research and Forecasting (WRF) model, simulates how ocean warming affects storm intensity.

The regional ocean model, based on the Finite Volume Coastal Ocean Model (FVCOM), simulates how sea level rise affects storm surge and overland inundation. The model-predicted peak surge levels are projected onto low-lying land areas to assess their impacts on coastal communities.

2.1 Regional Atmospheric Model

WRF is a non-hydrostatic, mesoscale atmospheric model (Skamarock et al. 2005), and has been widely used for hurricane simulations (e.g., Davis et al. 2008; Nolan et al. 2009a,b; Seroka et el. 2016). We configured triple-nested model domains for WRF (Fig. 2a). The outermost domain covers the western Atlantic at a coarse resolution of 12 km. The middle domain covers the south and middle Atlantic regions at a resolution of 4 km. The innermost domain uses a fine resolution of 1.33 km to resolve the Chesapeake Bay region. There are 40 vertical sigma levels. At the lateral boundaries of its outermost domain, WRF is forced by 6-hourly Final (FNL) operational global analysis data at 1^{o} spatial resolution (https://rda.ucar.edu/datasets/ds083.2/). At the ocean surface, WRF is forced by outputs from daily real-time global SST Sea Surface Temperature (SST) with 0.5^{o} resolution (hereafter RTG-SST, http://polar.ncep.noaa.gov/sst/rtg_low_res/). FNL is also used to initialize WRF at approximately 48 hours prior to the hurricane's landfall. Zhang et al. (2017) used this WRF model to simulate Hurricane Arthur (2014) and obtained good agreements between the predicted and observed storm track, storm intensity and forward propagation speed.

2.2 Regional Ocean Model

229 The unstructured-grid FVCOM was used to simulate storm surge and overland
230 inundation (Chen et al. 2003; 2006). The model domain covers Chesapeake Bay and the eastern
231 U.S. continental shelf (Fig. 2b). The horizontal resolution ranges from ~1 km in the inner shelf to
232 ~10 km near the open boundaries. The model resolves Chesapeake Bay and its surrounding lands
233 (up to 5 m height above the current mean sea level) at a resolution of 0.2-1.0 km. Finer
234 resolutions are placed over the City of Baltimore (5-10 m) (Fig. 2c) and the rural eastern shore of
235 Maryland including Dorchester County (100-200 m) (Fig. 2d), two focus areas in this study.
236 About 25% of the Chesapeake Bay shoreline is hardened, but these structures mostly use
237 shoreline stabilization techniques such as riprap and bulkheading and do not provide much
238 protection against flooding (Patrick et al. 2014; Palinkas et al. 2017). These small engineered
239 structures are not resolved in the FVCOM model. Neither are small-scale offshore engineered
240 structures such as bridge piers, breakwaters, and groynes.

241 The model is run in three-dimensional barotropic mode in which temperature and salinity are
242 kept constant. In the vertical direction, five sigma layers are used. At the offshore open boundary,
243 the sea level is prescribed using ten tidal constituents according to the Oregon State University
244 global tidal model TOPEX/POSEIDON 7.1 (Egbert and Erofeeva 2002). Hourly outputs of
245 surface wind and air pressure fields from WRF are used to drive FVCOM. A quadratic stress is
246 exerted at the bed, with the bottom roughness height set to be 2 mm in Chesapeake Bay and 2 cm
247 on the adjacent shelf (Lee et al. 2017). As a simplification the roughness heights are assumed to
248 be the same between the sea beds and the surrounding lands. We also ran the model with a
249 uniform roughness height and only found minor differences in the storm surge prediction.
250 FVCOM simulation started at about 1 week before a hurricane's landfall to give sufficient time
251 for the model to spin up.

252 To simulate overland inundation, coastal lands up to 5 m above the mean sea level are
253 included in the model domain. High-resolution (10 m horizontal resolution) digital elevation data
254 in land areas surrounding Chesapeake Bay are obtained from U.S. Geological Survey National
255 Elevation Dataset (Gesch 2009) while the elevation data (at a resolution of 1/3 arc-second) for
256 areas along the open coast are obtained from NOAA's Coastal Relief Model data (e.g. Grothe et
257 al. 2010). Bathymetry data are acquired from the NOAA 1 arc second resolution Bathymetric
258 Digital Elevation Model in estuaries, the 3 arc second Coastal Relief Model on the continental
259 shelf, and the 1 arc-minute ETOPO1 Global Relief Model in the deep ocean (Amante and Eakins
260 2009). Raw elevation and bathymetry data referenced to different vertical datum are converted to
261 the same vertical coordinate system (NAVD88) using the V-Datum program (Yang et al. 2008;
262 Lee et al. 2017).

263 Wetting and drying of grid cells is implemented to simulate overland inundation due to
264 storm surge and sea level rise. FVCOM uses a point treatment technique in which numerical
265 grids consist of wet and dry points with a boundary defined as an interface line between the
266 water and land respectively (Chen et al. 2011). A grid is treated as a wet point when the water
267 depth exceeds h_c (set to be 5 cm in our model), otherwise it is considered a dry point at which
268 velocities are set to zero.

269

270 *2.3 Design of numerical experiments*

271 To project the impact of climate change on coastal inundation in 2050 and 2100, we
272 make use of the Intergovernmental Panel on Climate Change fifth assessment report (IPCC AR5).
273 The IPCC AR5 projections are based on a set of greenhouse gas concentration scenarios called
274 Representative Concentration Pathways that reflect the updated greenhouse gas emission

reduction possibilities and climate change stabilization goals (Moss et al. 2010; van Vuuren et al. 2011). We selected RCP 4.5 and 8.5, representative of medium (delayed action) and high (growing) emission scenarios, respectively. The Coupled Model Intercomparison Project Phase 5 (CMIP5) used in the IPCC AR5 contains 15 General Circulation Models (GCMs). We extracted Sea Surface Temperature (SST) in the tropical Atlantic Ocean from these GCMs, and calculated the SST difference between the future climate and the historical reference period 1986-2005 (Villarini and Vecchi 2012). Then, the GCMs with minimum, median, and maximum SST changes were selected for the downscaling simulations. The median projection is for the SST to increase by 1.13 and 1.71 ºC at 2050 and by 1.48 and 2.94 ºC at 2100, with the lower values from RCP 4.5 and the higher values from RCP 8.5 (Table 1). The inter-model spread in SST is larger in 2100 than in 2050, reflecting larger uncertainty in the projection for the end of 21st century.

The GCMs are also used to project the future sea level rise, but local effects such as land subsidence and ocean dynamics in the northwest Atlantic Ocean are included. Church et al. (2013) analyzed individual contributions to sea level rise, and estimated the median values and likely ranges for projections of GMSL in the 21st century relative to 1986-2005. The median, lower and upper range of GMSL will be used to obtain the median, lower and upper range for the relative sea level rise in Chesapeake Bay. The regional land subsidence due to glacial isostatic adjustment was estimated following Miller et al. (2013). The regional sea level rise due to changing ocean dynamics was estimated according to Yin et al. (2009). Adding the three components together yielded the relative sea level rise in 2050 and 2100, as shown in Table 1. Our median estimate is nearly the same as Kopp et al. (2014)'s central estimate for the relative sea level rise in Chesapeake Bay while the lower (min) and upper (max) bounds correspond to

298 the two endpoints of their likely range (67% probability). In a recent study Kopp et al. (2017)
299 considered DP16 (DeConto and Pollard 2016) scenarios in which the rate of the sea level rise
300 would be much higher due to possible rapid loss of the polar ice sheets such as the deterioration
301 of Antarctic ice shelves. DP16 scenarios were not considered in this study. More detailed
302 information on the configuration of numerical experiments for climate change scenarios can be
303 found in Zhang and Li (2019).

304 We conducted a total of 13 numerical experiments. The control run was the hindcast
305 simulation of Hurricane Isabel (2003) which served as the baseline to assess the climate change
306 impacts. For Isabel, WRF was forced by the FNL operational global analysis data at the lateral
307 boundary and by daily RTG-SST at the ocean surface. For Isabel-like storms in 2050 and 2100,
308 WRF-FVCOM incorporated the effects of ocean warming and relative sea level rise under the
309 median, lower and upper range projections from RCP 4.5 and 8.5. Since the GCMs do not have
310 adequate resolutions to predict hurricanes in the future climate, they were not used to force WRF.
311 Instead WRF was forced by FNL at the lateral boundary. At the ocean surface, however, the
312 GCM's projected increase in the SST was added to RTG-SST to set the ocean surface boundary
313 condition for WRF. Following Hill and Lackmann (2011) and Mallard et al. (2013a), the GCM-
314 projected changes in the atmosphere temperature between the historical period and future climate
315 were averaged horizontally over the tropical Atlantic Ocean and then added to the FNL outputs
316 to set the initial and lateral boundary conditions for WRF (see also Zhang and Li 2019). This
317 approach provided a cost-effective alternative to running high-resolution regional climate models
318 (Knutson et al. 2013) and captures changes in the atmospheric thermal conditions (temperature
319 and moisture) associated with warmer SST. To account for the relative sea rise in FVCOM, the
320 projected increase in the mean sea level was superimposed onto the astronomical tides along the

open boundary of FVCOM. This is a simplified representation of the sea level rise, which changes coastlines gradually. To model geomorphic response to sea level rise, one would need to develop a coupled hydrodynamic-wave-sediment transport model to simulate shoreline erosion and deposition processes, but it is computationally prohibitive to run such a model for 50 and 100 years. One would also need to consider the role of coastal wetlands in shaping coastline changes under changing climate.

2.4 Inundation impact analysis

Google Map and Google Earth are used to visualize inundations over the land areas surrounding Chesapeake Bay, including City of Baltimore and Dorchester County in Maryland. Water level data from FVCOM were imported and overlaid on Google Map and Google Earth. Inundation depths were obtained by subtracting the digital elevation data from the water level in each grid cell. The result was a wet/dry profile of inundation. Google Earth allows users to add and view 3D buildings, thus enabling 3D views of inundations over buildings and structures.

A majority of the data used for the inundation impact analysis were collected from U.S. Census Bureau (https://www.census.gov/data.html) and housing websites such as Trulia (https://www.trulia.com) and Zillow (https://www.zillow.com). Dorchester County was chosen as a representative rural site. It is the largest county in Maryland and has a total area of 983 square miles (2,550 km^2). According to the census in 2010, the county had a population of 32,618 and a population density of 55 people per square mile (www.census.gov/quickfacts/dorchestercountymaryland, www.dorchestercountymd.com/). There were 14,681 housing units at an average density of 26 per square mile, with the average home value of $188,000. The average household size was 2.36 and the average family size was 2.86.

344 Model-predicted inundated areas for Dorchester County were combined with the census and
345 housing data to estimate numbers of houses and people affected by flooding. The total depth-
346 damage function for residential houses, which includes structure and content costs, was used to
347 estimate the flood damage, following the approach adopted by FEMA (Federal Emergency
348 Management Agency) HAZUS-MH (Hazards US for Multi-Hazard Earthquakes, Hurricanes and
349 Floods) program (Scawthorn et al. 2006a, b; Ding et al. 2008; HAZUS 2014).

350 The City of Baltimore was chosen as a representative urban site. It is the largest city in
351 Maryland, with a population of 2.81 million in the Baltimore metropolitan area. The city has a
352 total area of 92.1 square miles (239 km^2). Baltimore is densely populated, with approximately
353 7,671 people per square mile (https://www.census.gov/quickfacts/fact/table
354 /baltimorecitymaryland). Founded in 1729, Baltimore harbor is the second-largest seaport in the
355 Mid-Atlantic where millions of shipments are made every single year. Baltimore has about
356 50,800 firms where many of these firms and businesses are located on or near the waterfront. As
357 a large city, 93% of the homes in Baltimore are multi-unit buildings such as apartments, but a
358 majority of the properties in downtown Baltimore are commercial buildings. To estimate the
359 flood damage to Baltimore, we used the total depth-damage function appropriate for commercial
360 buildings, including structure and content costs (Scawthorn et al. 2006a, b; Smith 1994; Huizinga
361 et al. 2017). We did not index for future price increases/decreases in real estate. The purpose of
362 this inundation impact analysis is not to obtain a precise estimate for the economic loss caused
363 by coastal inundation but rather to examine relative changes in the storm surge damage due to
364 climate change.

365

366 **3. Results**

367 A hindcast simulation of Hurricane Isabel (2003) was conducted first and then compared
368 against simulations of a similar storm under the higher SST and sea level projected by the
369 climate models. The bay-wide response is presented first, followed by detailed analyses on
370 Dorchester County and City of Baltimore.

371

372 *3.1 Bay-wide response*

373 Hurricane Isabel made landfall at the Outer Bank of North Carolina on 18 September
374 2003, and travelled northwestward along a nearly-straight line that began 2 days before landfall
375 and lasted until its eventual dissipation over the Great Lakes. WRF accurately predicted Isabel's
376 track and forward propagation speed (Fig. 3a). The root-mean-square error (RMSE) between the
377 predicted and observed tracks is 29.3 km. The observed Minimum Sea Level Pressure (MSLP)
378 reached a low of 955 mb on late 17 September, but rebounded to 1000 mb on 19 September.
379 WRF captured the observed temporal evolution of storm intensity (Fig. 3b). Isabel attained a
380 maximum sustained wind (MSW) of 45 ms^{-1} at 10 m above the sea surface. This was well
381 simulated by WRF, although WRF slightly overestimated MSW post-landfall (Fig. 3c). The
382 RMSE for MSLP and MSW is 6.9 mb and 4.3 m s^{-1} respectively, while the correlation
383 coefficients are 0.94 and 0.96. The RMSE normalized by variances is 0.020/0.024 for MSLP/
384 MSW.

385 When exposed to warmer SST in the future climate, the storm intensifies. MSLP
386 decreases to a minimum of 952 mb in 2050 and 940-950 mb in 2100 (Fig. 3b). The MSLP
387 difference between the median RCP 4.5 and 8.5 projections is about 2 mb in 2050 but reaches 10
388 mb in 2100. MSW also becomes much stronger in the future climate: increasing from a peak

389 speed of 45 ms^{-1} during Isabel to ~50 ms^{-1} in 2050 and ~55 ms^{-1} in 2100 (Fig. 3c). Since the same
390 large-scale atmospheric flow fields (FNL) were used to force WRF at the lateral boundary, the
391 storm in the future climate follows essentially the same track as Hurricane Isabel (Fig. 3a).

392 The stronger storm results in higher storm surge. Together with sea level rise, high water
393 levels are generated in Chesapeake Bay. Two tidal gauge stations were selected for comparing
394 the sea level time series (their locations marked in Figure 2b). The Cambridge tidal gauge is
395 located in the mid-Bay, next to Dorchester County. The Baltimore tidal gauge is located next to
396 the Inner Harbor of downtown Baltimore. The observed peak surge height during Hurricane
397 Isabel was 1.6 m in Cambridge and 2.3 m in Baltimore. FVCOM accurately predicted the storm
398 surge: the RMSE is 0.15 m and the correlation coefficient is 0.97 (Figs. 4a and 4c). The
399 normalized RMSE is 0.035 in Cambridge and 0.040 in Baltimore. In 2050, the surge height is
400 ~2.1 m in Cambridge and ~2.7 m in Baltimore. The difference in the median projection of the
401 peak surge height between RCP 4.5 and RCP 8.5 is small, but the difference in the surge height
402 between the lower and upper range of RCP 4.5/8.5 is 0.28/0.27 m in Cambridge and 0.27/0.36 m
403 in Baltimore. Because the storm's forward propagation speed in 2050 is slightly slower than that
404 during Isabel (Fig. 3a), the storm surge reaches its peak water level 1-2 hours later at Cambridge
405 and Baltimore. More dramatic differences in the peak water level are found in the model
406 projections for 2100 (Figs. 4b and 4d). The peak water level from the median climate change
407 projections increases to 2.5/2.7 m (RCP 4.5/8.5) in Cambridge and 3.2/3.4 m (RCP 4.5/8.5) in
408 Baltimore. The spread among the model projections is considerably larger in 2100, with a surge
409 height difference of 0.6 m in Cambridge and 0.7 m in Baltimore under RCP 8.5.

410 The higher water levels lead to more extensive inundation around Chesapeake Bay (Fig.
411 5). During Hurricane Isabel, a large area on the eastern shore of Delmarva Peninsula was flooded,

412 as well as near-shore regions in the lower Chesapeake Bay and isolated spots on the western
413 shore of the northern Chesapeake Bay (Fig. 5a). These are low-lying land areas vulnerable to
414 coastal inundation. In 2050, the flooded areas expand from these regions (Figs. 5b and 5c). By
415 2100, flooding appears at many locations along the coastlines of Chesapeake Bay and its
416 tributaries, in addition to the eastern shore (Figs. 5d and 5e). Figure 5f compares the size of the
417 inundated areas between Hurricane Isabel and Isabel-like storms in the future climate. Isabel
418 flooded 1,850 km^2. A similar storm in 2050 floods 2,305/2,339 km^2 under the median projections
419 of RCP 4.5/8.5. By 2100, an Isabel-like storm floods 2,715 km^2 under RCP 4.5 median scenario
420 and 3,000 km^2 under RCP 8.5 median scenario, representing 47%-62% increase in the flooded
421 area over that during Hurricane Isabel. The total flooded area in 2100 varies from 2,674 to 3,359
422 km^2 between the upper and lower projections of RCP 8.5, representing $\pm$11% uncertainty around
423 the median projection. In comparison, a $\pm$5 cm error in the vertical datum would only result in
424 $\pm$3% differences in the inundation area. Most of the additional flooded areas are on the rural
425 eastern shore of Maryland and Virginia where agricultural fields and wetlands dominate the
426 landscape. The waterfront areas in cities like Norfolk, Washington, D.C., Annapolis and
427 Baltimore will be also be flooded, consisting mostly of commercial properties and apartment
428 buildings.

429 Additional calculations were done to separate the contributions of sea level rise and storm
430 surge to the total inundation area in the future climate. In 2050, sea level rise alone caused
431 599/688 km^2 to be flooded under the median projection of RCP 4.5/8.5. The additional inundated
432 areas caused by storm surge were 1,706/1,653 km^2, smaller than the area flooded by Isabel
433 (2003). A similar result was found for 2100: sea level rise flooded 1,184/1,484 km^2 under the
434 median RCP 4.5/8.5 projection and the storm surge flooded additional 1,531/1,586 km^2. The land

topography surrounding Chesapeake Bay rises more steeply away from the coastline, such that additional land areas flooded by storm surge would be smaller for the same surge height in the future climate.

3.2 Rural Dorchester County

Due to its shape, Dorchester County is known as heart of the Chesapeake (Fig. 6). Cambridge, the county seat with the highest population density, is located on the shore of the Choptank River in northern Dorchester County. The leaf-like parcel of land extends from Cambridge towards the main stem of Chesapeake Bay and is sandwiched between the Choptank River and the Little Choptank River. Along the coastline further south lies Taylor Island and Hooper Island. The Blackwater National Wildlife Refuge occupies the central part of southern Dorchester County. The refuge and the lands further south are low-lying areas vulnerable to coastal inundation. There are only a handful of major roads linking rural communities and fishing villages in Dorchester County, making emergency evacuation challenging.

When Hurricane Isabel hit in September 2003, the southern Dorchester County as well as parts of the leaf-like area in the northwest corner were flooded: the water depth was less than 0.5 m in the northwest but reached about 1.5 m over the Blackwater area (Fig. 7a). According to the median projections of RCP 4.5 and 8.5, the flooded areas show a modest expansion by 2050, because land elevation rises steeply further north (Figs. 7b and 7c). However, the inundation depth is significant higher. By 2100, the flooded areas expand towards higher grounds in the northeast direction (Figs. 7d and 7e). In addition, flooding appears along the banks of Choptank River and Nanticoke River (see Fig. 6 for their locations). More noticeably, water depth in the inundated areas is substantially higher, reaching 2.5-3 m in deepest places. Moreover, the

458 projected inundated areas and inundation depths are quite different in 2100 between RCP 4.5 and
459 8.5.

460 In 2100 there are substantial differences in the overland inundation among the GCMs in
461 each climate change scenario, reflecting larger uncertainty in climate projections at the end of
462 21st century (Fig. 8). The inundation depths display large differences among the lower range,
463 median and upper range of RCP 4.5 projections (Figs. 8a-8c). The inundation depths under RCP
464 8.5 are considerably larger than those under RCP 4.5, but show smaller differences among the
465 lower, median and upper projections (Figs. 8d-8f).

466 Figure 9 summarizes the total inundated area and average inundation depth for different
467 climate change scenarios. Hurricane Isabel was estimated to flood 825 km^2 in Dorchester County
468 (Fig. 9a). By 2050, the total inundated area in Dorchester County rises to ~885 km^2 under the
469 median projections of both RCP 4.5 and 8.5, with a range of 875 km^2 to 903 km^2 between the
470 lower and upper range of the climate model projections. By 2100, the total inundated area
471 increases to 919 km^2 under the median projection of RCP 4.5 and 942 km^2 under the median
472 projection of RCP 8.5. The range of the projected inundated area in Dorchester is smaller under
473 RCP 4.5 (42 km^2) than under RCP 8.5 (55 km^2). Flood damage typically increases
474 disproportionately with flood depth (Scawthorn et al. 2006a, b). The average inundation depth in
475 Dorchester County was just under 1.2 m during Hurricane Isabel, but increases to ~1.55 m under
476 the median projections of RCP 4.5 and 8.5 in 2050 (Fig. 9b). In 2100, the inundation depth
477 increases to 1.81 m under the median projection of RCP 4.5 and 2.02 m under the mean
478 projection of RCP 8.5, representing 51-68% increase in the inundation depth. Once again, the
479 spread in the inundation depth is smaller under RCP 4.5 (0.36 m) than under RCP 8.5 (0.49 m).

480 The model-predicted inundated areas were overlaid over the map of existing homes in
481 Dorchester County to estimate the total number of houses flooded during Hurricane Isabel and
482 Isabel-like storms in the future climate (Fig. 10a). Isabel flooded about 1,420 houses. Although
483 the storm in 2050 floods more land areas, it floods 80 less houses under the median projection of
484 RCP 4.5 because most of the additional flooded areas are not on residential areas and some of the
485 areas flooded by Isabel are not flooded by the storm in the future. However, the storm is
486 projected to flood about 1,740 houses under the high end projection of RCP 4.5. Although the
487 flooded area under the median projection of RCP 8.5 is only marginally larger than that under
488 the median projection of RCP 4.5, 420 more houses are flooded because the additional flooding
489 hit residential areas. By 2100, 1,850 houses are predicted to be flooded in Dorchester County
490 under the median projection of RCP 4.5 but over 2,190 houses are flooded under the median
491 projection of RCP 8.5. There are large differences in the number of flooded houses (~400-500
492 houses) between the high and low ends of climate model projections under both RCP 4.5 and
493 RCP 8.5, suggesting larger uncertainty in predicting flooded houses in 2100.

494 With an average home size of 1500 ft^2 in Dorchester County, we can estimate flood
495 damage to residential buildings by using the depth-damage function (Scawthorn et al. 2006a, b;
496 HAZMAT 2014), as shown in Fig. 10b. Because the model does not have the spatial resolution
497 to resolve each house and lot, we used the mean inundation depth in the flooded areas to obtain
498 an estimate for the property damage. The damage to residential houses was estimated to be
499 ~$100 million during Hurricane Isabel and would increase to $109/143 million in 2050 and
500 $183/216 million in 2100 under RCP4.5/8.5. Combing the housing data with the census data, we
501 estimated that the flooding due to Hurricane Isabel directly affected about 3,351 people. Under

502 the median climate change projections, a similar storm affects 3,162/4,106 people (RCP 4.5/RCP
503 8.5) in 2050 and 4,366/5,168 people (RCP 4.5/RCP 8.5) in 2100.

504

505 *3.3 City of Baltimore*

506 Downtown Baltimore is situated next to the Inner Harbor which is connected to Patapsco
507 River, a tributary of Chesapeake Bay (Fig. 11). Hundreds of businesses are found in the
508 downtown financial district, including skyscrapers like the Bank of America building and the
509 Baltimore World Trade Center. Both Charles Street and Pratt Street are significant avenues of
510 commercial and cultural activity. The Inner Harbor itself is the chief commercial and tourist
511 destination in Baltimore, visited by over 13 million people a year. It is home to museums such as
512 the Maryland Science Center, the National Aquarium in Baltimore and the Flag House & Star-
513 Spangled Banner Museum. To the west of the Inner Harbor are the Light street and Charles
514 Street where land elevation rises rather rapidly. South of the Inner Harbor lies museums, Federal
515 Hill Park and apartment buildings. North of the Inner Harbor lies in Pratt Street and business
516 buildings. To the north-east of the Inner Harbor lies in Fells Point and Little Italy featuring
517 residential buildings and restaurants, with many low-lying areas.

518 When Hurricane Isabel hit in 2003, it flooded streets around the Inner Harbor (Fig. 12a),
519 with Pratt Street and Light Street as well as streets in Fells Point and Little Italy under water. The
520 predicted inundated area is in agreement with anecdotal reports of flooding in Baltimore (e.g. Fig.
521 1a). In 2050, the flooded area expands west of Light Street and north of Pratt Street, and covers a
522 large area in Little Italy and Fells Point, according to the median projection of RCP 8.5 (Fig.
523 12b). In 2100, the flooding reaches Charles Street in the west and 2 blocks north of Pratt Street
524 (Fig. 12c). Several blocks in Little Italy and Fells Point are also flooded. The total inundated area

525 in Baltimore was 2.2 km^2 during Hurricane Isabel, increases to 5.1 km^2 in 2050 under the median
526 projections of RCP 4.5 and 8.5, and expands ~4 times to 8.1/9.1 km^2 under RCP 4.5/8.5 in 2100
527 (Fig. 13a). Interestingly, the average inundation depth was about 1.13 m during Isabel but
528 reduces slightly to 1-1.12 m under all climate change scenarios in 2050 (Fig. 13b). The flooded
529 areas during Hurricane Isabel were low-lying land right at the water front. As more areas are
530 flooded in 2050, the land elevation rises such that the averaged inundation depth is smaller even
531 though the peak water level is higher. In 2100, as more land areas are flooded, the inundation
532 depth increases to 1.17/1.28 m under the median projection of RCP 4.5/8.5. The inundation
533 depth also expands a wider range in 2100 under RCP 8.5, with the largest inundation depth at
534 1.51 m and the smallest inundation depth at 1.15 m.

535 How do these inundated areas translate to potential economic loss to the City of
536 Baltimore? First the google map was used to calculate the percentage (the total square footage)
537 of the flooded areas that are occupied by buildings. Then the total depth-damage function for
538 commercial buildings, expressed in terms of a unit cost per m^2 (Huizinga et al. 2017), was used
539 to estimate the flood cost to these buildings. Again we use the total damage function that
540 includes the structure and content costs. We estimated a loss of $29 million in downtown
541 Baltimore during Hurricane Isabel (Fig. 14). It is further assumed that the property values are
542 indexed in today's dollars, given the difficulty in forecasting future price movements in real
543 estate. In 2050, the estimated economic cost due to an Isabel-like storm is estimated to be $98
544 million under RCP 4.5 but $100/$115 million under the median/high end projections of RCP 8.5
545 (Fig. 14). This represents 3-4 fold increases in the economic damage to downtown Baltimore.
546 There are relatively small differences in the estimated damage ($94 - $115 million) among
547 different climate change scenarios and different climate models. By 2100, the economic loss

increases to $150/$162 million under the median projections of RCP 4.5/8.5 (Fig. 14). The highest end projection of RCP 8.5 results in a total economic loss of $173 million to the City of Baltimore. This represents nearly 6 times increase in the property damage, with huge economic consequences. The estimated flood damage in 2100 varies from $102 to $162 million, depending on whether the low or upper projection of RCP 4.5 is used in the calculations. It ranges from $152 to $173 million under RCP 8.5.

4. Discussion and Conclusion

Using the climate model projections to drive regional atmosphere-ocean models, we have investigated how ocean warming and sea level rise affect storm surge and coastal inundation in Chesapeake Bay. Warming ocean produces more intense storms and stronger winds, resulting in higher storm surge and more extensive flooding. Hurricane Isabel (2003) generated a peak water level of 1.6 m in Cambridge and 2.2 m in Baltimore, Maryland. By 2100, the peak water level is projected to reach 2.5/2.7 m in Cambridge and 3.2/3.4 m in Baltimore under RCP 4.5/8.5. The net increase of 0.9/1.1 m in Cambridge is slightly larger than the projected sea level rise of 0.85/1.06 m. However, in the upper-estuary location Baltimore, the peak water level increases by 1.0/1.2 m under RCP 4.5/8.5, representing 18%/13% over the sea level rise. In terms of overland inundation, Isabel flooded 1,850 km^2. By 2100, an Isabel-like storm floods 2,715 km^2 under RCP 4.5 median scenario and 3,000 km^2 under RCP 8.5 median scenario. Sea level rise alone flooded 1,184/1,484 km^2 under RCP 4.5/8.5, and the storm surge flooded additional 1,531/1,586 km^2. Our modeling study has illustrated the nonlinear effects of sea level rise, storm surge and land topography on coastal inundation.

570 The rural and urban areas show quite different responses to climate change, due to
571 differences in land topography and geography. Over the rural Dorchester County, the inundated
572 area shows moderate expansion in the future climate but the average inundation depth is ~30%
573 higher in 2050 and ~50%-70% higher in 2100. The number of houses flooded increases from
574 1,420 during Hurricane Isabel to 1,850/2,190 in 2100 under the climate change scenario RCP
575 4.5/8.5. The estimated total flood damage in Dorchester County increases from $100 million in
576 2003 to $183/$216 million in 2100 under the median projection of RCP 4.5/8.5. In comparison,
577 the inundated area in the City of Baltimore is projected to expand four-fold: the flooded area was
578 estimated to be 2.2 km^2 during Hurricane Isabel, and is projected to expand to 5.1 km^2 in 2050
579 and 8.1/9.1 km^2 in 2100 under RCP 4.5/8.5. Given the intense economic activities in the water
580 front areas in Downtown Baltimore, these large expansions of the inundated areas would
581 translate to larges increases in economic damages. The estimated property loss increases from
582 $29 million in 2003 to $100 million in 2050 and $150/$162 million in 2100 under RCP 4.5/8.5.
583 There are uncertainties in projecting future coastal inundation impacts and economic damage due
584 to uncertainties in climate change scenarios and inter-model differences among climate models.
585 In 2100 the estimated property damage ranges from $132 million to $231 million in Dorchester
586 County. It ranges from $102 million to $173 million in downtown Baltimore.
587 One limitation of this study is the assumption of uniform relative sea level rise. The rates
588 of land subsidence in Chesapeake Bay are spatially variable. For example, by 2100 the relative
589 sea level rise in Norfolk is projected be 10 cm larger than that in Baltimore and Washington,
590 D.C., which is about 10% of the sea level rise (Boesch et al. 2018). Ralston et al. (2019)
591 reconstructured bathymetry changes in the Hudson River between 1860s and 2016 using
592 historical charts. A similar approach could be used to consider the effects of variable land

593 subsidence in Chesapeake Bay. Instead of the historical charts, we would need projections of
594 vertical land motion for the 21st century.

595 In this study we focused on Category 2 Hurricane Isabel (2003) and its cousins in the
596 future climate because Isabel was considered as a 100-year flooding event for planning purposes
597 by cities and towns around Chesapeake Bay. To obtain a comprehensive assessment of flood
598 risks, however, we would need to model storms of various return periods (say 10-100 years). The
599 probabilistic approach to sea level rise projections (Kopp et al. 2014, 2017) would naturally fit
600 into this risk assessment. To generate an ensemble of storms appropriate for probabilistic
601 calculations, one would need to analyze the past storm climatology and consider how climate
602 change might affect the storm climatology. It is computationally expensive to conduct these
603 model runs. Many previous studies represented storms with the parametric wind model using
604 parameters such as the central pressure deficit, the storm size, the forward propagation speed, the
605 storm heading and the landfall location, and employed Joint Probability Method (JPM)-Optimal
606 Sampling (OS) schemes to select representative storms (Toro et al. 2010a, b; Niedoroda et al.
607 2010; Condon and Sheng 2012). Others used a statistical deterministic hurricane model
608 (Emanuel et al. 2006) to generate synthetic storms under the large-scale atmospheric and oceanic
609 environments projected by GCMs (Lin et al. 2012, 2016). These hurricane models are
610 computationally efficient, but they cannot capture mesoscale wind structures and wind speed
611 asymmetry in hurricanes and produce accurate wind predictions needed for accurate storm surge
612 predictions. Short-term storm-surge forecasts now use mesoscale atmospheric models to forecast
613 winds, and our study is one of the few that use such a model to obtain realistic simulations of
614 hurricanes under changing climate conditions. The feasibility of our approach has been
615 demonstrated. With increasing computational power, it could be used to obtain a probabilistic

risk assessment of coastal inundation in the future climate. The inundation maps obtained from this modeling approach would be more realistic than the traditional floodplain maps generated from the parametric wind model.

Many fringe areas of Chesapeake Bay are covered by salt marshes which are not simulated in our model. Coastal wetlands may defend coastal communities from storm surge and sea level rise, and mitigate coastline erosion (Reza et al. 2016; Kirwan et al. 2016; Rezaie et al. 2020). During storm floods, drag in vegetation on wetlands decelerates water flows and reduces marsh erosion. It would be interesting to consider these dynamic interactions between storm-induced flows and vegetation in a future study. An intermediate step might be to prescribe a drag coefficient using empirically determined Manning's coefficient to represent different types of vegetative surfaces such as coastal wetlands, forests and farms (Bunya et al. 2010; Dietrich et al. 2011; Ferreira et al. 2014). As sea level rises, coastal morphology continually adapts toward equilibrium and salt marsh might migrate upstream. An integrated modeling system, consisting of submodels of hydrodynamics, surface waves, sediment transport (e.g. Warner et al. 2010; Xie et al. 2018), ecogeomorphology (Lesser et al. 2004; Nardin and Edmonds 2014) and engineered shoreline structures (Ge et al. 2012), would need to be developed in order to simulate the evolving coastlines and coastal inundation under changing climate.

When assessing potential economic damages due to coastal flooding, we used simple depth-damage functions. This depth-damage approach does not include potential wave damage, although waves are relatively weak in semi-enclosed bays and estuaries such as Chesapeake Bay. Future work could consider cost-benefit analysis of various mitigation and adaptation measures in reducing inundation impacts, following similar approaches as Neumann et al. (2015) and Diaz (2016) among others. Zhang and Li (2019) compared the storm surge height in Chesapeake Bay

between two model runs: one soft shoreline scenario which allows low-lying areas to be flooded; one hard shoreline scenario which prevents flooding at the current coastline. They found that hardening shorelines would increase the surge height in the upper parts of the estuary by 0.5 m. A future extension of this work could examine different shoreline scenarios such as adaptation measures in low-lying rural areas and installation of engineered structures around urban infrastructure. The costs of flood damage could then be compared against the costs of the mitigation and adaptation measures to identify most cost-effective ways to bolster coastal resiliency in the entire region.

Data Availability:

The inundation graphics are hosted at http://geronimo.hpl.umces.edu/mingli/. Model output is available at https://doi.org/10.5281/zenodo.3497531.

653 **References:**

654 Amante C, Eakins BW (2009) ETOPO1 Global Relief Model converted to PanMap layer format,
655 NOAA-Natl. Geophys. Data Cent., Boulder, Colo., doi:10.1594/pangaea.769615.
656 Bengtsson L, Botzet M, Esch M (1996) Will greenhouse-induced warming over the next 50 years
657 lead to higher frequency and greater intensity of hurricanes? Tellus 48A: 57–73.
658 Bilskie MV, Hagen SC**,** Alizad KA, Medeiros SC, Passeri DL, Needham H (2016) Dynamic
659 simulation and numerical analysis of hurricane storm surge under sea level rise with
660 geomorphologic changes along the northern Gulf of Mexico. Earth's Future 4(5): 177-193.
661 Boesch DF et al. (2018) Sea-level Rise: Projections for Maryland 2018, 27 pp. University of
662 Maryland Center for Environmental Science, Cambridge, MD.
663 Bunya S, Dietrich JC, Westerink JJ et al. (2010) A high resolution coupled riverine flow, tide,
664 wind, wind wave and storm surge model for southern Louisiana and Mississippi: Part I —
665 model development and validation. Monthly Wea. Rev. 138: 345–377.
666 Chen C, Liu H, Beardsley RC (2003) An unstructured grid, finite-volume, three-dimensional,
667 primitive equations ocean model: application to coastal ocean and estuaries. J. Atmos. &
668 Oceanic Tech. 20: 159-186.
669 Chen C, Beardsley RC, Cowles G (2006) An unstructured grid, finite-volume coastal ocean
670 model (FVCOM) system. Oceanogr. 19(1): 78–89.
671 Chen C et al. (2011) An unstructured-grid, finite-volume community ocean model fvcom user
672 manual (3rd edition), SMAST/UMASSD-11-1101, 315 pp.
673 Chen C, and Coauthors (2013) Extratropical storm inundation testbed: Intermodel comparisons
674 in Scituate, Massachusetts. J. Geophys. Res. Ocean 118: 5054-5073,
675 doi:10.1002/jgrc.20397.
676 Condon AJ, Sheng PY (2012) Evaluation of coastal inundation hazard for present and future
677 climates. Nat. Hazards 62: 345-373.
678 Church J A et al. (2013) Sea level change. In Stocker TF et al.(ed) Climate Change 2013: The
679 Physical Science Basis. Contribution of Working Group I to the Fifth Assessment Report of
680 the Intergovernmental Panel on Climate Change, Cambridge Univ. Press, pp. 1137–1216,
681 Church JA, White NJ (2011) Sea-level rise from the late 19th to the early 21st century. Survey
682 Geophys. 32: 585-602.

683 Dangendorf S, Marcos M, Wöppelmann G, Conrad CP, Frederikse T, Riva R (2017)
684 Reassessment of 20th century global mean sea level rise.
685 PNAS,https://doi.org/10.1073/pnas.1616007114
686 Davis C et al. (2008) Prediction of landfalling hurricanes with the Advanced Hurricane WRF
687 model. Mon. Wea. Rev. 136: 1990-2005.
688 DeConto RM, Pollard D (2016) Contribution of Antarctica to past and future sea-level rise.
689 Nature 531: 591-597.
690 Diaz DB (2016). Estimating global damages from sea level rise with the Coastal Impact and
691 Adaptation Model (CIAM). Climatic Change 137(1-2): 143-156.
692 Dietrich JC, Zijlema M, Westerink JJ et al. (2011). Modeling hurricane waves and storm surge
693 using integrally-coupled, scalable computations. Coastal Engineering 58: 45-65,
694 DOI:10.1016/j.coastaleng.2010.08.001.
695 Dinan T (2017). Projected increases in hurricane damage in the United States: The role of
696 climate change and coastal development. Ecol. Econ. 138:186-198.
697 Ding A, White JF, Ullman PW, Fashokun AO (2008) Evaluation of HAZUS-MH flood model
698 with local data and other program. Nat. Hazards Rev. 9(1):20-28.
699 Domingues CM, Church JA, White NJ, Gleckler PJ, Wijffels SE, Barker PM, Dunn JR (2008)
700 Improved estimates of upper-ocean warming and multi-decadal sea-level rise. Nature 453:
701 1090-1093.
702 Domingues R, Goni G, Baringer M, Volkov D (2018) What caused the accelerated sea level
703 changes along the United States East Coast during 2010-2015? Geophy. Res. Lett.:
704 https://doi.org/10.1029/2018GL081183.
705 Egbert GD, Erofeeva SY (2002). Efficient inverse modeling of barotropic ocean tides. J. Atmos.
706 & Oceanic Tech., 19(2): 183-204.
707 Eichler TP, Gaggini N, Pan Z (2013) Impacts of global warming on Northern Hemisphere winter
708 storm tracks in the CMIP5 model suite. J. Geophys. Res.-Atmosphere 118(10): 3919-32.
709 El-Sabh MI (1990) Statistical analysis of long-term storm surge data, storm surge: observation
710 and modeling. Proceedings of International Symposium on Storm Surge. China Ocean Press,
711 Beijing, China: 313-314.
712 Emanuel KA (2006) Climate and tropical cyclone activity: A new model downscaling approach.
713 J. Climate 19: 4797–4802.

714 Emanuel KA, Ravela S, Vivant E, Risi C (2006) A statistical deterministic approach to hurricane
715 risk assessment. Bull. Amer. Meteor. Soc. 87: 299-314.
716 Emanuel KA (2008) The Hurricane-Climate Connection. Bull. Amer. Meteor. Soc. 89*:* ES10-
717 ES20.
718 Emanuel KA (2013) Downscaling CMIP5 climate models shows increased tropical cyclone
719 activity over the 21st century. Proc. the Nat. Acad. Sci.
720 www.pnas.org/cgi/doi/10.1073/pnas.1301293110.
721 Engelhart SE, Horton BP, Douglas BC, Peltier WR, Törnqvist TE (2009) Spatial variability of
722 late Holocene and 20th century sea level-rise along the Atlantic coast of the United State.
723 Geology 37: 1115-18.
724 Ezer T (2013) Sea level rise, spatially uneven and temporally unsteady: Why the U.S. East
725 Coast, the global tide gauge record and the global altimeter data show different trends.
726 Geophys. Res. Lett. 40(20): 5439-5444.
727 Ezer T, Atkinson LP, Corlett WB, Blanco JL (2013) Gulf Stream's induced sea level rise and
728 variability along the U.S. mid-Atlantic coast. J. Geophys. Res. Oceans 118: 685–697.
729 Ezer T, Corlett WB (2012) Is sea level accelerating in the Chesapeake Bay? A demonstration of
730 a novel new approach for analyzing sea level data. Geophys. Res. Lett. 39: L19065,
731 doi:10.1029/2012GL053435.
732 Familkhalili R, Talke SA (2016) The effect of channel deepening on tides and storm surge: A
733 case study of Wilmington, NC. Geophys. Res. Lett., 43: 9138-47,
734 doi:10.1002/2016GL069494.
735 Ferreira CM, Irish JL, Olivera F (2014) Uncertainty in hurricnae surge simulation due to land
736 cover specification. J. Geophys. Res. Oceans 119: 1812-27, doi:10.1002/2013JC009604.
737 Ge, J, Chen C, Qi J, Ding P, Beardsley (2012) A dike-groyne algorithm in a terrain-following
738 ocean model (FVCOM): development, validation and application. Ocean Modeling 47:26-
739 41.
740 Gesch DB (2009) Analysis of Lidar elevation data for improved identification and delineation of
741 lands vulnerable to sea level rise. J. Coast. Res. 53: 49–58.
742 Grothe P, Taylor LA, Eakins BW, Warnken RR, Carignan KS, Lim E, Caldwell RJ, Friday DZ
743 (2010). Digital elevation model of Ocean City, Maryland: procedures, data sources, and
744 analysis. NOAA Tech. Memo. NESDIS NGDC-37, Dept. of Commerce, Boulder, Colo., 37

745 pp.
746 Hagen SC, Bacopoulos P (2012) Synthetic storms contributing to coastal flooding in Florida's
747 Big Bend Region with application to sea level rise. Terr. Atmos. Ocean. Sci. 23(5): 481–
748 500.
749 Hallegatte S, Green C, Nicholls RJ, Corfee-Morlot J (2013) Future flood losses in major coastal
750 cities. Nat. Clim. Change 3(9): 802–806.
751 Hauer ME, Evans JM, Mishra DR (2016) Millions projected to be at risk from sea-level rise in
752 the continental Unites States. Nature Climate Change, doi: 10.1038/NCLIMATE2961.
753 Hay CC, Morrow E, Kopp RE, Mitrovica JX (2015) Probabilistic reanalysis of twentieth-century
754 sea-level rise. Nature 517:481–484.
755 HAZUS (2014) The Federal Emergency Management Agency's (FEMA's) methodology for
756 estimating potential losses from diasters. http://www.fema.gov/hazus/.
757 Hill KA, Lackmann GM (2011) The impact of future climate change on TC intensity and
758 structure: A downscaling approach. Journal of Climate 24(17): 4644-61.
759 Hinkel J, Vuuren Dp, Nicholls RJ, Klein RJT (2013) The effects of miigation and adaptation on
760 coastal impacts in the 21st century. Clim. Change 117: 783394.
761 Hinkel J et al. (2014) Coastal flood damage and adaptation costs under 21st century sea-level rise.
762 Proc. Natl. Acad. Sci. U.S.A. 111(9): 3292–3297.
763 Holleman RC, Stacey MT (2014) Coupling of sea level rise, tidal amplification, and inundation.
764 J. Phys. Oceanogr., 44(5): 1439–1455.
765 Horsburgh, KJ, Wilson C (2007) Tide-surge interaction and its role in the distribution of surge
766 residuals in the North Sea. J. Geophy. Res. Oceans 112: C08003, doi:10.1029/2006JC004033.
767 Huizinga J, Moel H. de Szewczyk W. (2017). Global flood depth-damage functions.
768 Methodology and the database with guidelines. EUR 28552 EN. doi: 10.2760/16510.
769 IPCC (2013) Climate Change 2013: The Physical Science Basis. Working Group I Contribution
770 to the IPCC 5th Assessment Report - Changes to the Underlying Scientific/Technical
771 Assessment (IPCC-XXVI/Doc.4).
772 Kerr P C and Coauthors (2013) US IOOS coastal and ocean modeling testbed: Inter- model
773 evaluation of tides, waves, and hurricane surge in the Gulf of Mexico. J. Geophys. Res.
774 Ocean 118: 5129-5172, doi:10.1002/jgrc.20376.

775 Kirwan ML, Walters DC, Reay WG, Carr JA (2016) Sea level driven marsh expansion in a
776 coupled model of marsh erosion and migration. Geophys. Res. Lett. 43: 4366–4373,
777 doi:10.1002/ 2016GL068507.
778 Knutson TR et al. (2013) Dynamical downscaling projections of twenty-first-century Atlantic
779 hurricane activity: CMIP3 and CMIP5 model-based scenarios. J. Climate 26(17): 6591-6617.
780 Knutson TR, Tuleya RE (2004) Impact of CO2-induced warming on simulated hurricane
781 intensity and precipitation: Sensitivity to the choice of climate model and convective
782 parameterization. J. Climate 17: 3477–3495.
783 Kopp RE (2013) Does the mid-Atlantic United States sea level acceleration hot spot reflect
784 ocean dynamic variability? Geophys. Res. Lett. 40(15): 3981-3985.
785 Kopp RE et al. (2014) Probabilistic 21st and 22nd century sea-level projections at a global
786 network of tide gauge sites. Earth's Future 2: 287–306.
787 Kopp RE et al. (2017) Implications of Antarctic ice-cliff collapse and ice-shelf hydrofracturing
788 mechanisms for sea-level projections. Earth's Future 5: 1217-1233.
789 Kulp S, Strauss BH (2017) Rapid escalation of coastal flood exposure in US municipalities from
790 sea level rise. Climatic Change, doi:10.1007/s10584-017-1963-7.
791 Lee SB, Li M, Zhang F (2017) Impact of sea level rise on tidal range in Chesapeake and
792 Delaware Bays. J. Geophys. Res.-Oceans 122(5): 3917-3938.
793 Lesser G, Roelvink J, Van Kester J, Stelling G (2004) Development and validation of a three-
794 dimensional morphological model. Coast. Eng. 51: 883– 915.
795 Li M, Zhong L, Boicourt WC, Zhang S, Zhang DL (2006) Hurricane-induced storm surges,
796 currents and destratification in a semi-enclosed bay. Geophys. Res. Lett. 33: L02604,
797 doi:10.1029/2005GL024992.
798 Li M, Zhong L, Boicourt WC, Zhang S, Zhang DL (2007) Hurricane-induced destratification and
799 restratification in a partially-mixed estuary. J. Mar. Res. 65: 169-192.
800 Lin N, Emanuel K, Oppenheimer M, Vanmarcke E (2012) Physically based assessment of
801 hurricane surge threat under climate change. Nature Climate Change 2(6): 462.
802 Lin N, Kopp RE, Horton BP, Donnelly JP (2016) Hurricane Sandy's flood frequency increasing
803 from year 1800 to 2100. Proc. the National Acad. of Sci. 113(43): 12071-12075.
804 Lowe JA, Gregory JM (2005) The effects of climate change on storm surges around the United
805 Kingdom. Phil. Trans. of the Royal Soc. of London A363(1831): 1313-1328.

806 Mallard MS, Lackmann GM, Aiyyer A, Hill K (2013a) Atlantic hurricanes and climate change.
807 Part I: experimental design and isolation of thermodynamic effects. J. Climate 26(13): 4876-
808 4893.
809 Mallard MS, Lackmann GM, Aiyyer A (2013b) Atlantic hurricanes and climate change. Part II:
810 role of thermodynamic changes in decreased hurricane frequency. J. Climate 26(21): 8513-
811 8528.
812 McAlpine SA, Porter JR (2018) Estimating recent local impacts of sea-level rise on current
813 real-estate losses: A housing market case study in Miami-Dade, Florida. Popul. Res. &
814 Policy Rev. 37:871-895.
815 McNamara DE, Gopalakrishnan S, Smith MD, Murray AB (2015) Climate Adaptation and
816 Policy-Induced Inflation of Coastal Property Value. PLoS One 10, e0121278.
817 Marcos M, Calafat FM, Berihuette A, Dangendorf S (2015) Long-term variations in global sea
818 level extremes. J. Geophys. Res.-Oceans: 120, 8115-34, doi:10.1002/2015JC011173.
819 McInnes KL, Walsh KJE, Hubbert GD, Beer T (2003) Impact of sea-level rise and storm surges
820 on a coastal community, Nat. Hazards 30(2): 187–207.
821 Mikhailova MV (2011) Interaction of Tides and Storm Surges at the Elbe River Mouth. Water
822 Res. 38(3): 284–297.
823 Miller KG, Kopp RE, Horton BP, Browning JV, Kemp AC (2013) A geological perspective on
824 sea-level rise and its impacts along the US mid-Atlantic coast. Earth's Future 1(1): 3-18.
825 Mitchell M, Hershner C, Herman J, Schatt D, Mason P, Eggington E (2012) Recurrent flooding
826 study for tidewater Virginia. Report of the Virginia Institute of Marine Science to the
827 Governor and the General Assembly of Virginia.
828 Moftakhari HR, AghaKouchak A, Sanders BF, Feldman DL, Sweet W, Matthew RA, Luke
829 A(2015) Increased nuisance flooding along the coasts of the United States due to sea level
830 rise: Past and future. Geophys. Res. Lett. 42: 9846–9852.
831 Moss RH et al. (2010) The next generation of scenarios for climate change research and
832 assessment. Nature 463: 747-756.
833 Mousavi ME, Irish JL, Frey AE, Olivera F, Edge BL (2011) Global warming and hurricanes: the
834 potential impact of hurricane intensification and sea level rise on coastal flooding. Climatic
835 Change 104(3-4): 575-597.

836 Nardin W, Edmonds DA (2014) Optimum vegetation height and density for inorganic
837 sedimentation in deltaic marshes. Nature Geoscience, doi:10.1038/ngeo2233.
838 Neumann J, Hudgens D, Herter J, Martinich J (2011) The economics of adaptation along
839 developed coastlines. Clim. Change 2: 89-98, doi:10.1002/wcc.90.
840 Neumann J, Emanuel K, Ravela S, Ludwig L, Kirshen P, Bosma K, Martinich J (2015) Joint
841 effects of storm surge and sea-level rise on US Coasts: new economic estimates of impacts,
842 adaptation, and benefits of mitigation policy. Climatic Change, 129:337-349.
843 Niedoroda AW, Resio DT, Toro GR, Divoky D, Das HS, Reed CW (2010) Analysis of the
844 coastal Mississippi storm surge hazard. J. Ocean Eng., doi:10.1016/j.oceaneng.2009.08.019.
845 Nicholls RJ (2004) Coastal flooding and wetland loss in the 21st century:changes under the SRES
846 climate and socio-economic scenarios. Glob. Environ. Change 14(1): 69-86.
847 Nolan DS, Zhang JA, Stern DP (2009a) Evaluation of planetary boundary layer
848 parameterizations in tropical cyclones by comparison of in situ observations and high-
849 resolution simulations of Hurricane Isabel (2003). Part I: Initialization, maximum winds,
850 and the outer-core boundary layer. Mon. Wea. Rev. 137: 3651-3674.
851 Nolan DS, Zhang JA, Stern DP (2009b) Evaluation of planetary boundary layer
852 parameterizations in tropical cyclones by comparison of in situ observations and high-
853 resolution simulations of Hurricane Isabel (2003). Part II: Inner-Core Boundary Layer and
854 Eyewall Structure. Mon. Wea. Rev. 137: 3675–3698.
855 Orton P et al. (2015) New York city panel on climate change 2015 report: Dynamic coastal flood
856 modeling. Ann. N. Y. Acad. Sci. 1336(1): 56–66.
857 Orton P, Conticello F, Cioffi F, Hall T, Georgas N, Lall U, Blumberg A, MacManus K (2018)
858 Hazard assessment from storm tides, rainfall and sea level rise on a tidal river estuary. Nat.
859 Hazards: 1-29.
860 Palinkas CM, Sanford LP, Koch EW (2017) Influence of shoreline stabilization structures on the
861 nearshore sedimentary environment in mesohaline Chesapeake Bay. Estuaries & Coasts,
862 https://doi.org/10.1007/s12237-017-0339-6.
863 Patrick CJ, Weller DE, Li X, Ryder M (2014) Effects of shoreline alteration and other stressors
864 on submerged aquatic vegetation in subestuaries of Chesapeake Bay and the Mid-Atlantic
865 coastal bays. Estuaries & Coasts 37: 1516-31, doi: 10.1007/s12237-014-9768-7.
866 Peng M, Xie L, Pietrafesa LJ (2004) A numerical study of storm surge and inundation in the

867 Croatan–Albemarle–Pamlico Estuary System. Est., Coast. Shelf Sci. 59: 121-137,
868 doi:10.1016/j.ecss.2003.07.010.
869 Piecuch CG, Bittermann K, Kemp AC, Ponte RM, Little CM, Engelhart SE, Lentz SJ (2018)
870 River-discharge effects on United States Atlantic and Gulf coast sea-level changes. PNAS,
871 115 (30), 7729-7734, doi/10.1073/pnas.1805428115
872 Ralston DK, Talke SA, Geyer WR, Al- Zubaidi HAM, Sommerfield CK (2019) Bigger Tides,
873 Less Flooding: Effects of Dredging on Barotropic Dynamics in a Highly Modified Estuary. J.
874 Geophys. Res. Oceans. doi:10.1029/2018JC014313.
875 Reza M, Orton PM, Georgas N, Blumberg AF (2016) Three-dimensional hydrodynamic
876 modeling of storm tide mitigation by coastal wetlands. Coastal Engineering 111: 83-94.
877 Rezaie AM, Loerzel J, Ferreira CM (2020), Valuing natural habitats for enhancing coastal
878 resilience: Wetlands reduce property damage from storm surge and sea level rise. PLoS ONE
879 15(1):e0226275. https://doi.org/10.1371/journal.pone.0226275.
880 Sallenger A, Doran KS, Howard PA (2012) Hotspot of accelerated sea-level rise on the Atlantic
881 coast of North America. Nature Climate Change 2: 884-88.
882 Scawthorn C et al. (2006a) HAZUS-MH flood loss estimation methodology. I: Overview and
883 flood hazard characterization. Nat. Hazards Rev. 7(2): 60–71.
884 Scawthorn C et al. (2006b) HAZUS-MH Flood loss estimation methodology. II: Damage and
885 loss assessment. Nat. Hazards Rev. 7(2): 72–81.
886 Scheffner NW, Fitzpatrick PJ (1997) Real-time predictions of surge propagation. In Estuarine
887 and Coastal Modeling, M. L. Spaulding, and A. F. Blumberg, ED.. Amer. Soc. of Civ. Eng.
888 374-388.
889 Seroka G, Miles T, Xu Y, Kohut J, Schofield O, Glenn S (2016) Hurricane Irene sensitivity to
890 stratified coastal ocean cooling. Mon. Wea. Rev. 144: 3507-3530.
891 Shen J, Wang HV, Sisson M, Gong W (2006) Storm tide simulation in the Chesapeake Bay
892 using an unstructured grid model. Est., Coast. Shelf Sci. 68(1-2): 1-16.
893 Skamarock WC, Klemp J, Dudhia J, Gill DO, Barker D, Duda MG, Powers JG (2008) A
894 Description of the Advanced Research WRF Version 3. NCAR Technical Note NCAR/TN-
895 475+STR.
896 Smith, DI (1994) Flood damage estimation – A review of urban stage-damage curves and loss
897 functions. Water SA Vol. 20 No. 3 July 1994. ISSN 0378-4738.

898 Smith JM, Cialone MA, Wamsley TV, McAlpin TO (2010) Potential impact of sea level rise on
899 coastal surges in southeast Louisiana. Ocean Eng. 37(1): 37-47.
900 Spanger-Siegfried E, Fitzpatrick MF, Dahl K (2014) Encroaching tides: How sea level rise and
901 tidal flooding threaten U.S. East and Gulf Coast communities over the next 30 years.
902 Cambridge, MA: Union of Concerned Scientists.
903 Sweet W, Park J. (2014) From the extreme to the mean: Acceleration and tipping points of
904 coastal inundation from sea level rise. Earth's Future 2: 579–600.
905 Talke, SA, Orton P, Jay DA (2014) Increasing storm tides in New York Harbor, 1944-2013.
906 Geophys. Res. Lett. 41: 3149-55, doi:10.1002/2014GL059574.
907 Toro G, Niedoroda AW, Divoky D, Reed CW (2010a) Quadrature-based approach for the
908 efficient calculation of surge hazard. J. Ocean Eng., doi:10.1016/j.oceaneng.2009.09.005.
909 Toro G, Resio DT, Divoky D, Niedoroda AW, Reed CW (2010b) Efficient joint probability
910 methods for hurricane surge frequency analysis. J. Ocean Eng.,
911 doi:10.1016/j.oceaneng.2009.09.004.
912 USGCRP (2017) Climate Science Special Report: Fourth National Climate Assessment, Volume
913 I, edited by Wuebbles DJ et al. U.S. Global Change Research Program, Washington, DC,
914 USA, 470 pp.
915 Vecchi GA, Soden BJ (2007) Global warming and the weakening of the tropical circulation. J.
916 Climate 20(17): 4316-4340.
917 Villarini G, Vecchi GA (2012) Twenty-first-century projections of North Atlantic tropical storms
918 from CMIP5 models. Nature Climate Change 2(8): 604-607.
919 Van Vuuren et al. (2011) The representative concentration pathways: an overview. Climatic
920 Change 109: 5-31.
921 Warner JC, Armstrong B, He R., Zambon JB (2010) Development of a Coupled Ocean-
922 Atmosphere-Wave-Sediment Transport (COAWST) modeling system. Ocean Modeling 35
923 (3): 230-244.
924 Woolings T, Gregory JM, Pinto JG, Reyers M, Brayshaw DJ (2012) Response of the North
925 Atlantic storm track to climate change shaped by ocean-atmosphere coupling. Nature
926 Goescience 5: 313-17.

927 Woth K, Weisse R, von Storch H (2006) Climate change and North Sea storm surge extremes: an
928 ensemble study of storm surge extremes expected in a changed climate projected by four
929 different regional climate models. Ocean Dyn. 56(1): 3–15.
930 Wu S-Y, Najjar R, Siewert J (2009) Potential impacts of sea-level rise on the Mid- and Upper-
931 Atlantic region of the United States. Climate Change 95: 121-138.
932 Xie X, Li M, Ni W (2018) Roles of wind-driven currents and surface waves in sediment
933 resuspension and transport during a tropical storm. J. Geophys. Res, DOI:
934 10.1029/2018JC014104.
935 Yang Z, Myers EP, Wong AM, White SA (2008) VDatum for Chesapeake Bay, Delaware Bay
936 and adjacent coastal water areas: Tidal datums and sea surface topography, NOAA
937 Technical Report NOS CS 15, 110 pp., NOAA, Silver Spring, MD.
938 Yang Z et al (2014). A modeling study of coastal inundation induced by storm surge, sea-level
939 rise, and subsidence in the Gulf of Mexico. Nat. Hazards 71(3): 1771–1794.
940 Yin J, Goddard PB (2013) Oceanic control of sea level rise patterns along the East Coast of the
941 United States. Geophys. Res. Lett. 40(20): 5514-5520.
942 Yin J, Griffies SM, Stouffer RJ (2010) Spatial variability of sea level rise in twenty-first century
943 projections. J. Climate 23(17): 4585–4607.
944 Yin J, Schlesinger ME, Stouffer RJ (2009) Model projections of rapid sea-level rise on the
945 northeast coast of the United States. Nature Geoscience 2(4): 262.
946 Zervas C (2001) Sea level variations of the United States, 1854-1999, NOAA Technical Report
947 NOS CO-OPS 36.
948 Zervas C (2009) Sea level variations of the United States 1854–2006. *NOAA Technical Report*
949 *NOS CO-OPS*, *53*.
950 Zhang F, Li M, Ross AC, Lee SB, Zhang DL (2017) Sensitivity Analysis of Hurricane Arthur
951 (2014) Storm Surge Forecasts to WRF Physics Parameterizations and Model Configurations.
952 Weather & Forecasting 32(5): 1745-1764.
953 Zhang F, Li M (2019) Impacts of ocean warming, sea level rise and coastline management on
954 storm surge in a semi-enclosed Bay. J. Geophys. Res. 124,
955 https://doi.org/10.1029/2019JC015445.
956 Zhong L, Li M, Zhang DL (2010) How do uncertainties in hurricane model forecasts affect
957 storm surge predictions in a semi-enclosed bay? Est., Coast. & Shelf Sci. 90(2): 61-72.

958

959

960 **Table Caption:**

961

962 Table 1. Projected increases in sea surface temperature (SST) in the Atlantic Ocean and relative
963 sea level rise in Chesapeake Bay. The 'median', 'minimum', and 'maximum' scenarios are
964 based on the median value and likely lower and upper bounds of projected global mean sea
965 level rises in the IPCC AR5 report.

966

967 **Figure Captions:**

968

969 Figure 1. Photos of flooding scenes in (a) Baltimore and (b) Dorchester County, MD during
970 Hurricane Isabel (2003). (c) Model-predicted inundated areas around Chesapeake Bay
971 region during Isabel.

972 Figure 2. (a) Triple-nested WRF model domains (denoted by the thick black boxes) with
973 resolutions of 12, 4, and 1.33 km. (b) FVCOM model grids (red) in which the two yellow
974 dots mark the locations of tidal gauge stations in Cambridge and Baltimore, MD. Zoomed-
975 in view of fine-resolution FVCOM grids for (c) the City of Baltimore and (d) Dorchester
976 County, MD.

977 Figure 3. (a) Hurricane tracks, time series of (b) minimum sea level pressure (MSLP) and (c)
978 maximum sustained wind speed (MSW) for Hurricane Isabel in 2003 (black) and Isabel-like
979 storms in 2050 (thin lines) and 2100 (thicker lines). Open circles mark the observed MSLP
980 and MSW during Hurricane Isabel. Green/red lines represent the median climate projections
981 in RCP4.5/8.5.

982 Figure 4. Storm surge generated at Cambridge, MD (left, a and b) and Baltimore, MD (right, c
983 and d) by Hurricane Isabel (2003) and Isabel-like storms in 2050 (a, c) and 2100 (b, d). The
984 open circles represent the observed surge during Isabel and the black line represents the

985 model prediction. The green/red lines represent the water level projection under the median
986 condition in RCP 4.5/8.5 while the shades represent the spreads among the GCM models.
987 Figure 5. (a)-(e) Flooded areas (red) around Chesapeake Bay during Hurricane Isabel (a) and
988 Isabel-like storms in 2050 (b, c) and 2100 (d, e) (the present day water surface in
989 Chesapeake bay is shown as blue). (f) Total flooded area during Hurricane Isabel and under
990 different climate change scenarios.
991 Figure 6. Geographic map of Dorchester County, Maryland.
992 Figure 7. Model predicted inundated area in Dorchester County, MD during Hurricane Isabel (a)
993 and Isabel-like storms in 2050 (b, c) and 2100 (d, e) under the median projections of RCP
994 4.5 (b, d) and RCP 8.5 (c, e).
995 Figure 8. Model predicted inundated area in Dorchester County, MD during Isabel-like storms in
996 2100 under the lower (left), median (middle), and upper (right) projections of RCP 4.5 (top)
997 and RCP 8.5 (bottom).
998 Figure 9. The total inundated area and the average water depth over the inundated land in
999 Dorchester County, MD for Hurricane Isabel (2003) and Isabel-like storm in 2050 and 2100
1000 under RCP 4.5 and 8.5.
1001 Figure 10. (a) Number of houses affected by flooding and (b) estimated property damage in
1002 Dorchester County due to Hurricane Isabel (2003) and Isabel-like storm in 2050 and 2100
1003 under RCP 4.5 (green) and RCP 8.5 (red) scenarios.
1004 Figure 11. Map of downtown Baltimore, Maryland. The thick black box marked the area shown
1005 in Figure 12.
1006 Figure 12. Model predicted inundated area in Baltimore, MD during Hurricane Isabel (a) and
1007 Isabel-like storms in 2050 (b) and 2100 (c) under the median projection of RCP 8.5.

1008 Figure 13. The total inundated area (a) and the average water depth (b) over the inundated land in
1009 the City of Baltimore, MD for Hurricane Isabel (2003) and Isabel-like storm in 2050 and
1010 2100 under RCP 4.5 and 8.5.
1011 Figure 14. Estimated flood damage to commercial buildings in the City of Baltimore based on
1012 the depth-damage function.
1013
1014

Figure 1

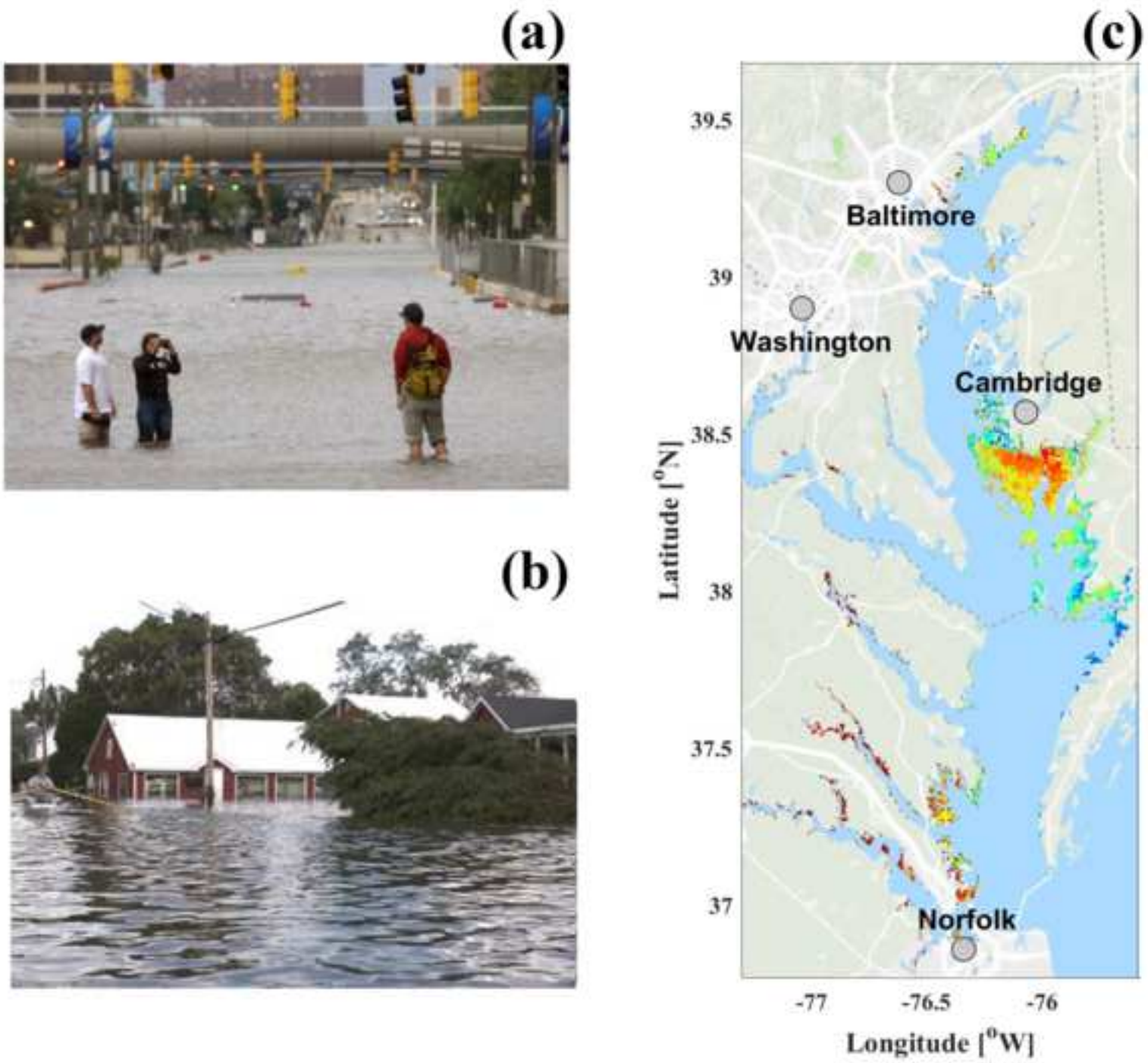

Figure 2

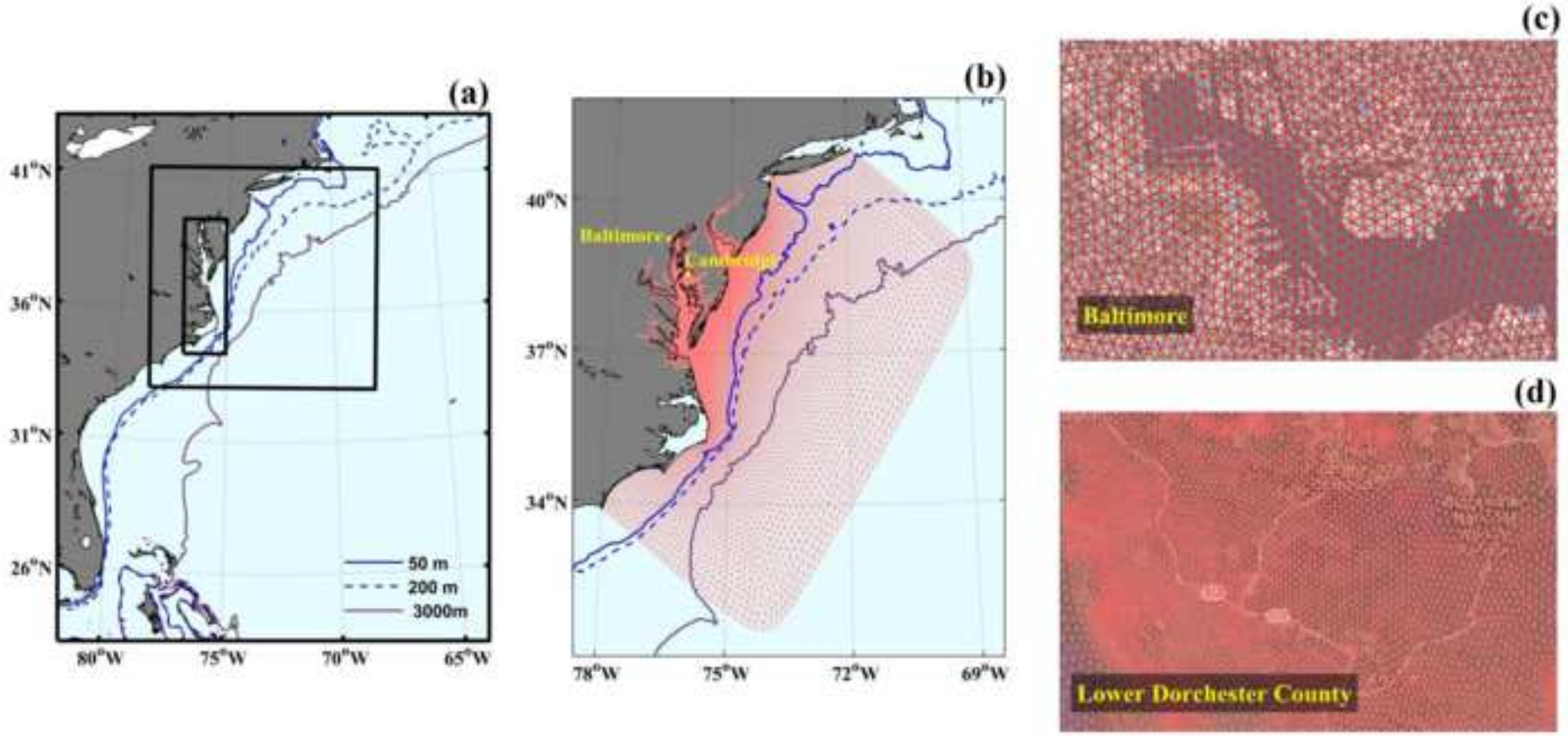

Figure 3

Click here to access/download;Figure;fig3.tif

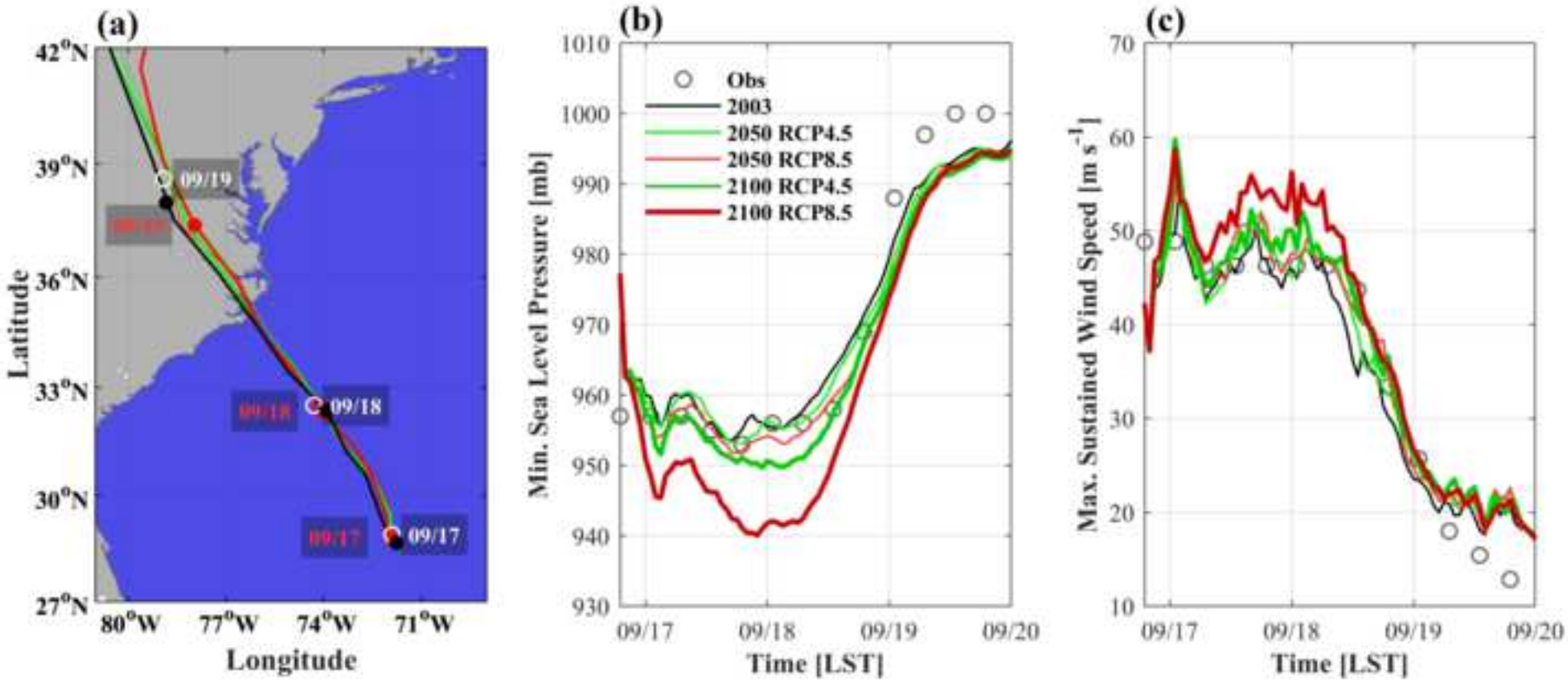

Figure 4

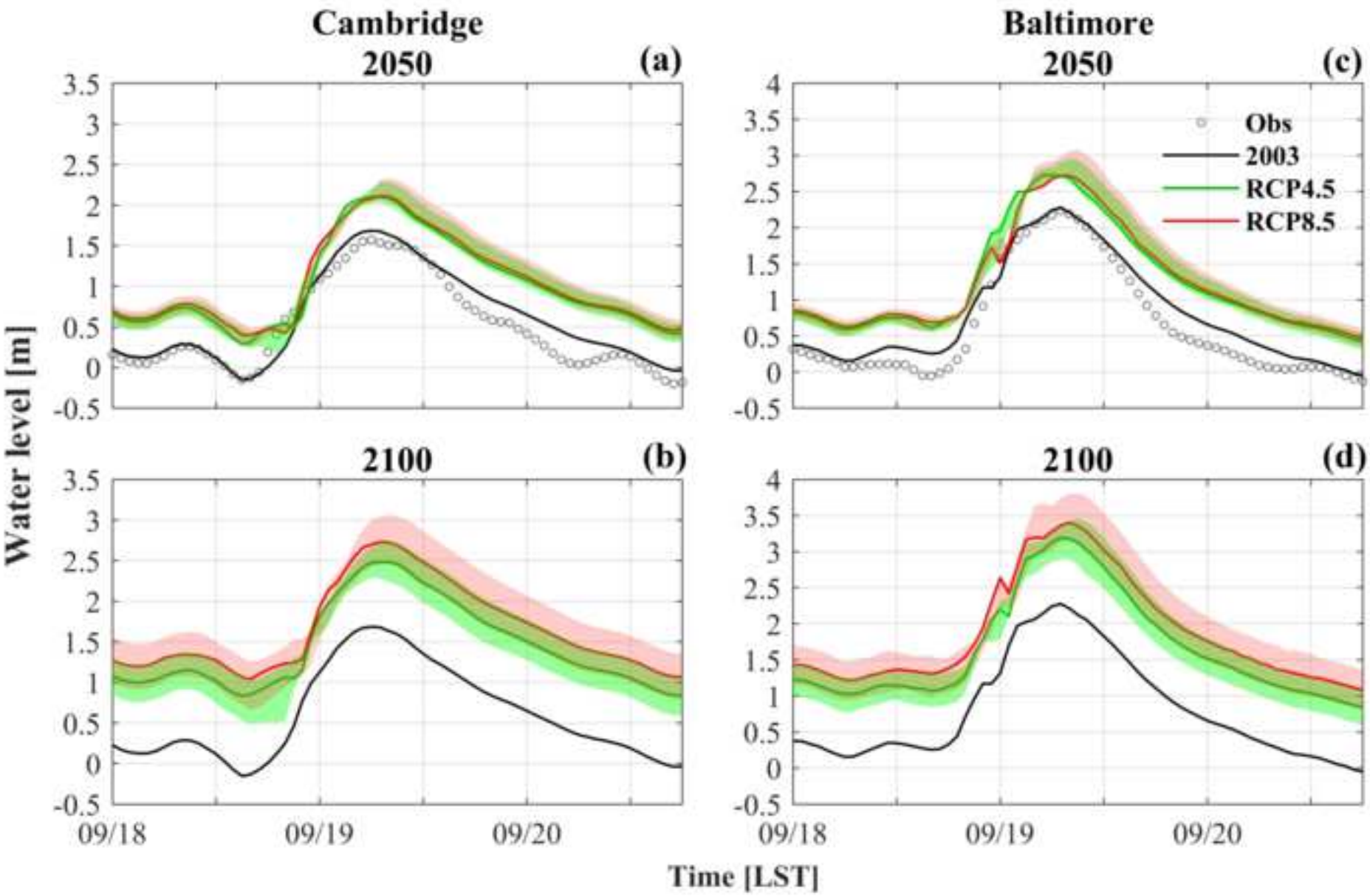

Figure 5

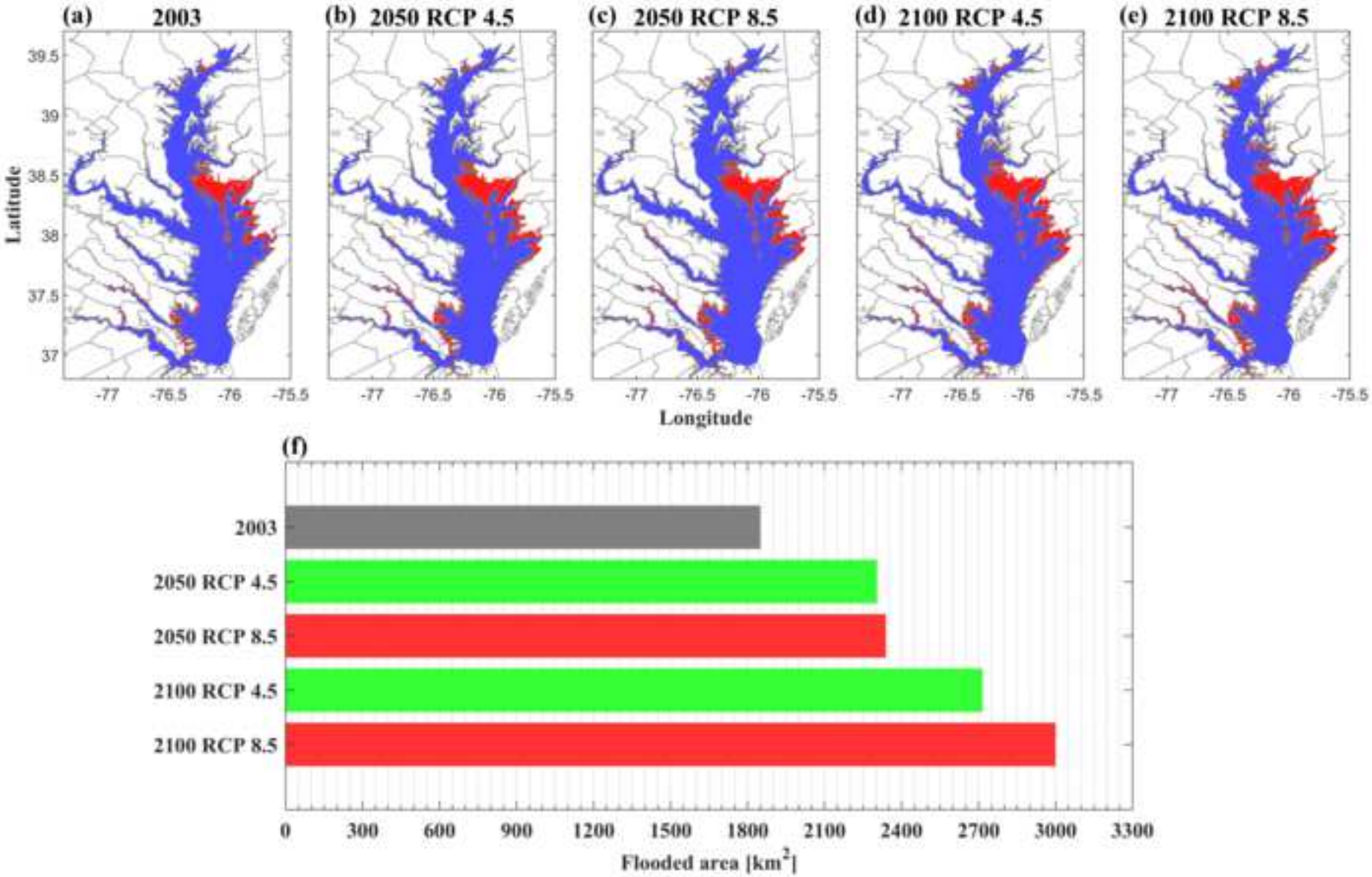

Figure 6

Click here to access/download;Figure;fig6.tif

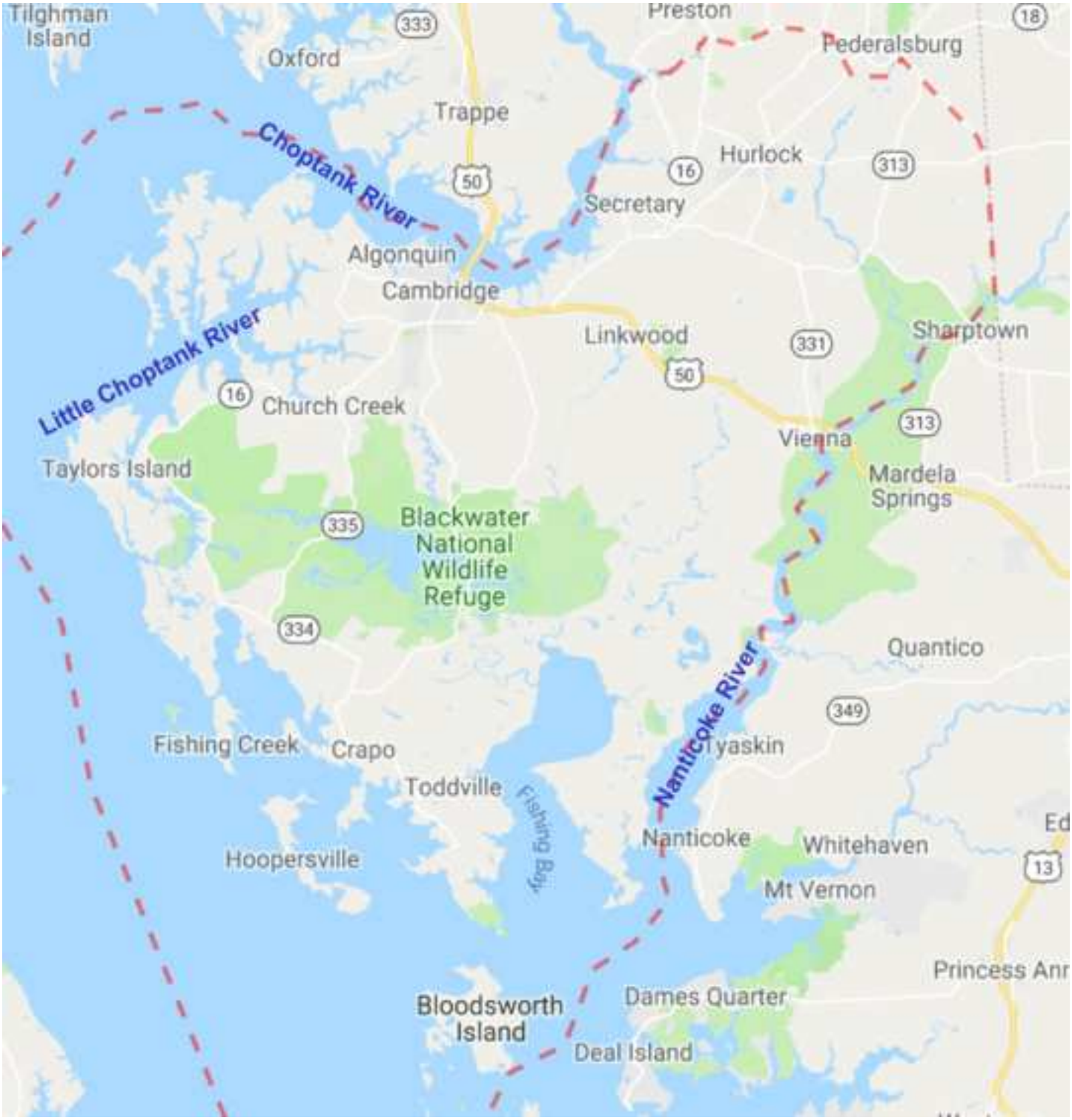

Figure 7

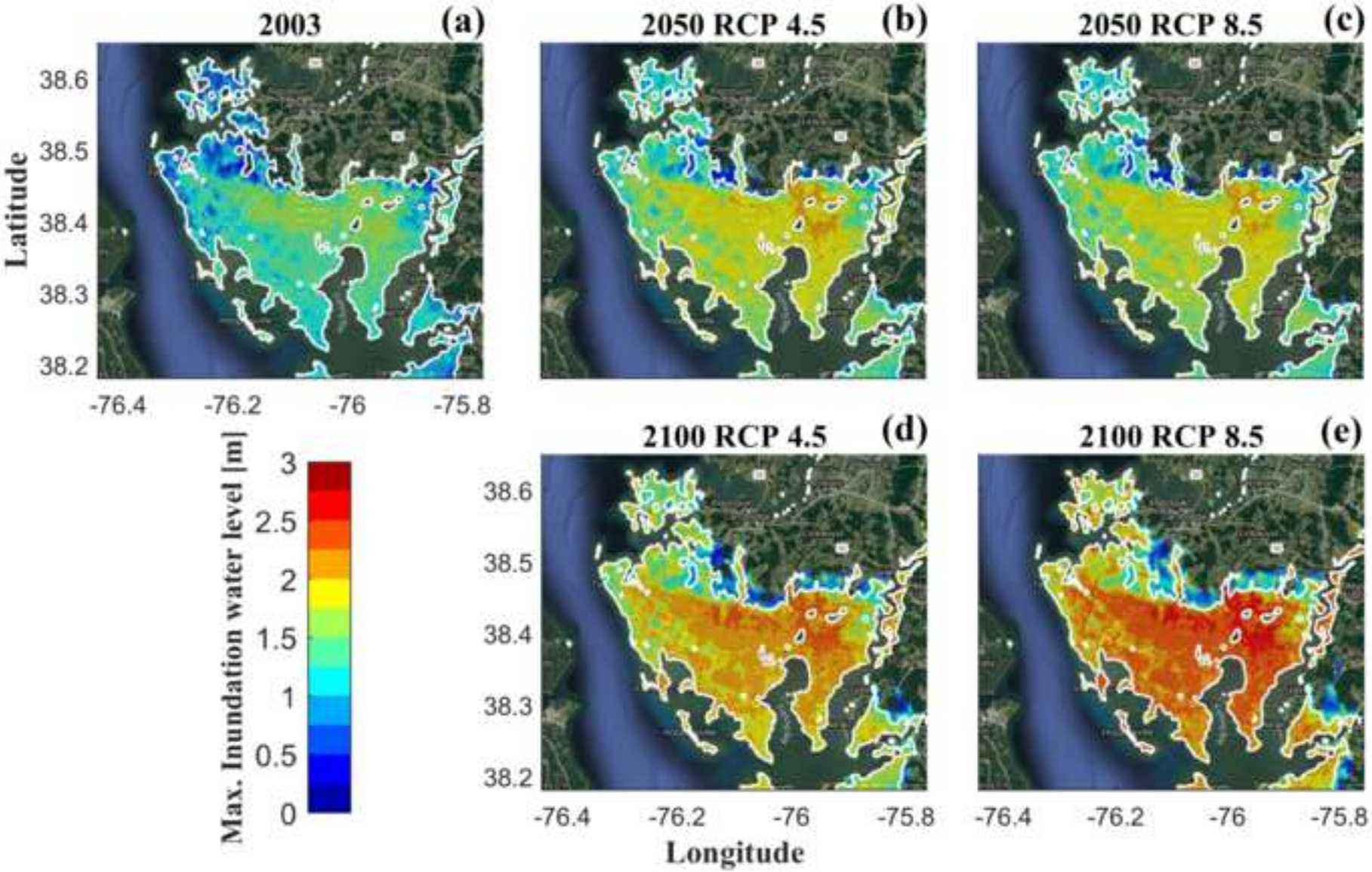

Figure 8

Click here to access/download;Figure;fig8.tif

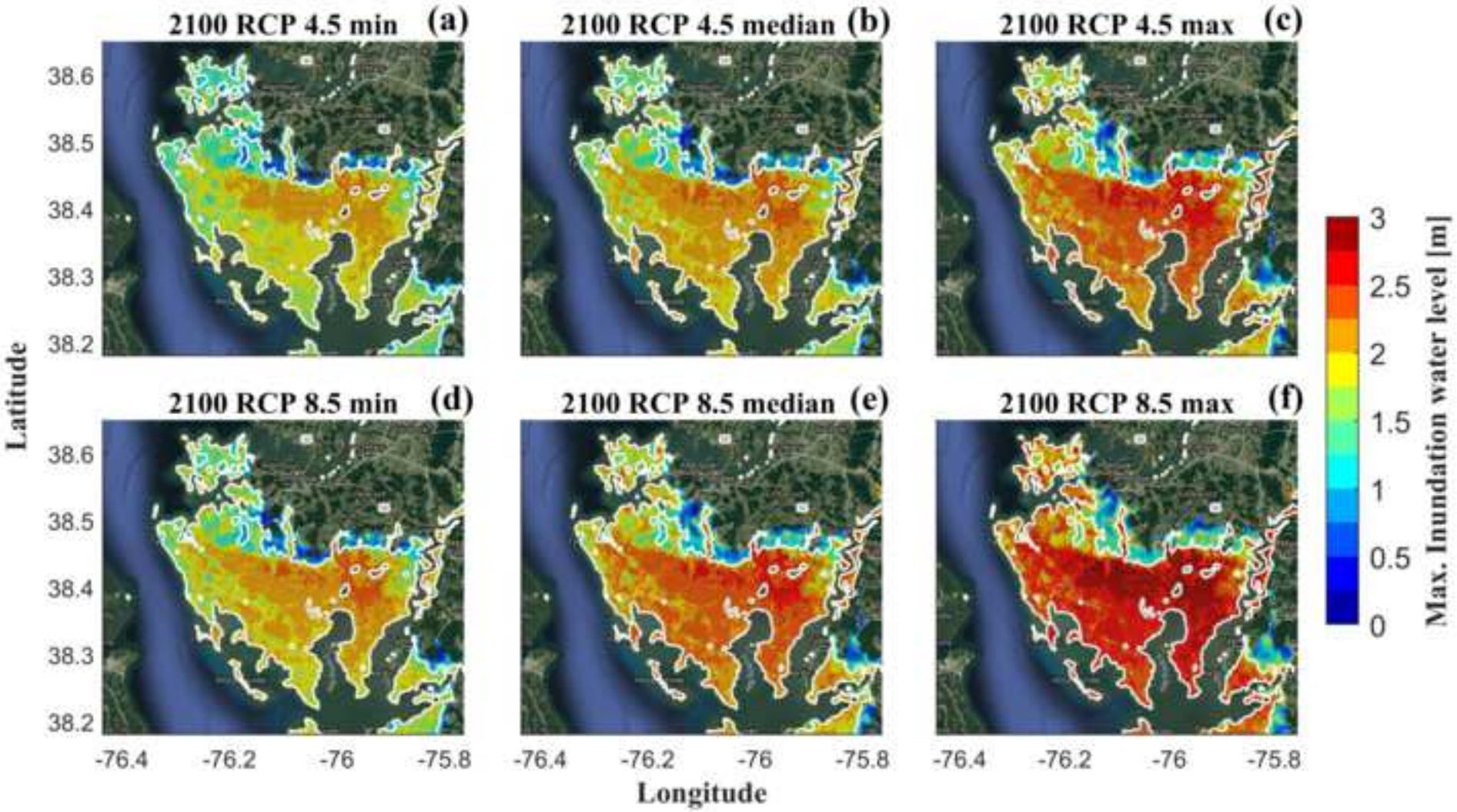

Figure 9

Click here to access/download;Figure;fig9.tif

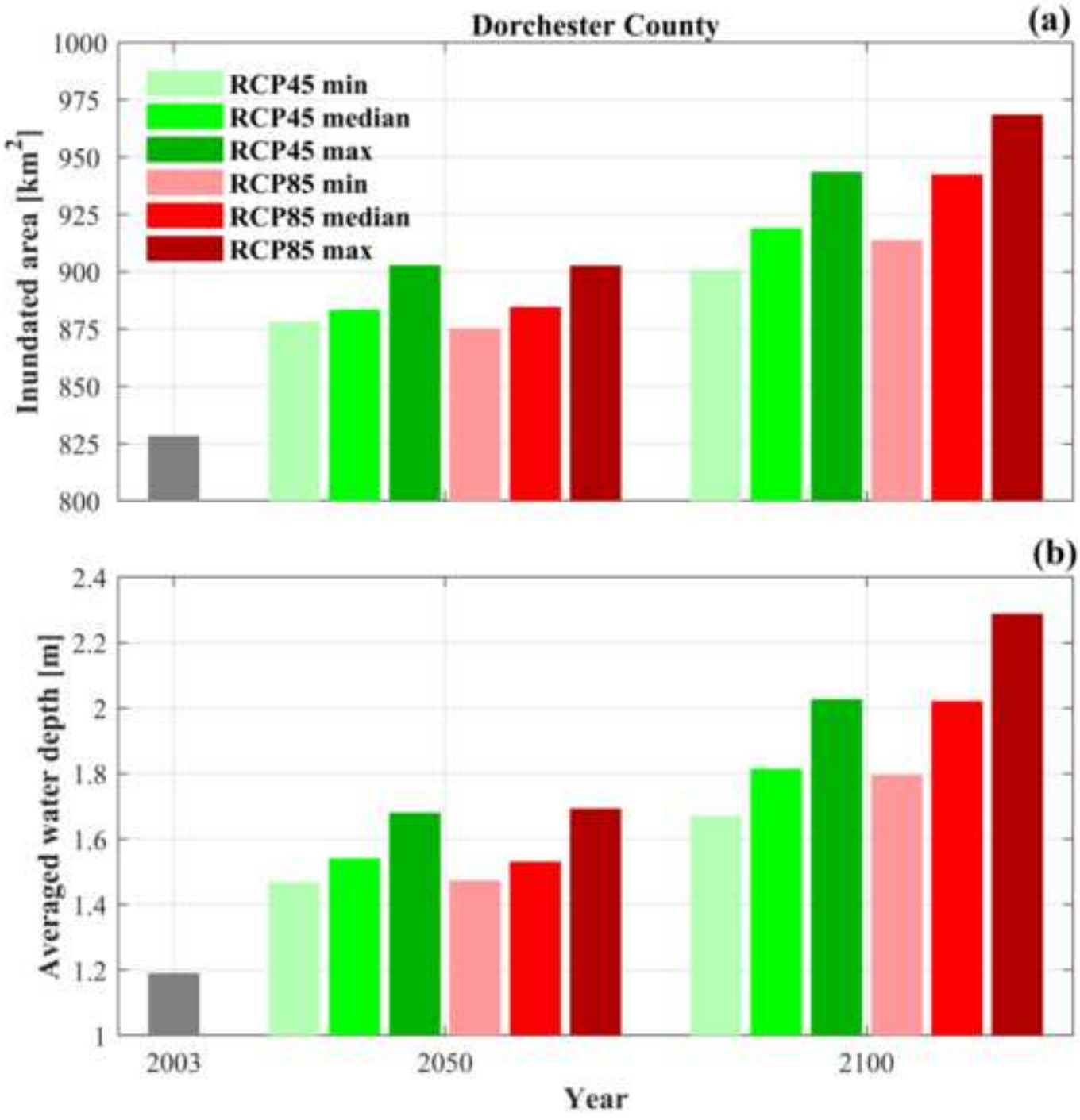

Figure 10

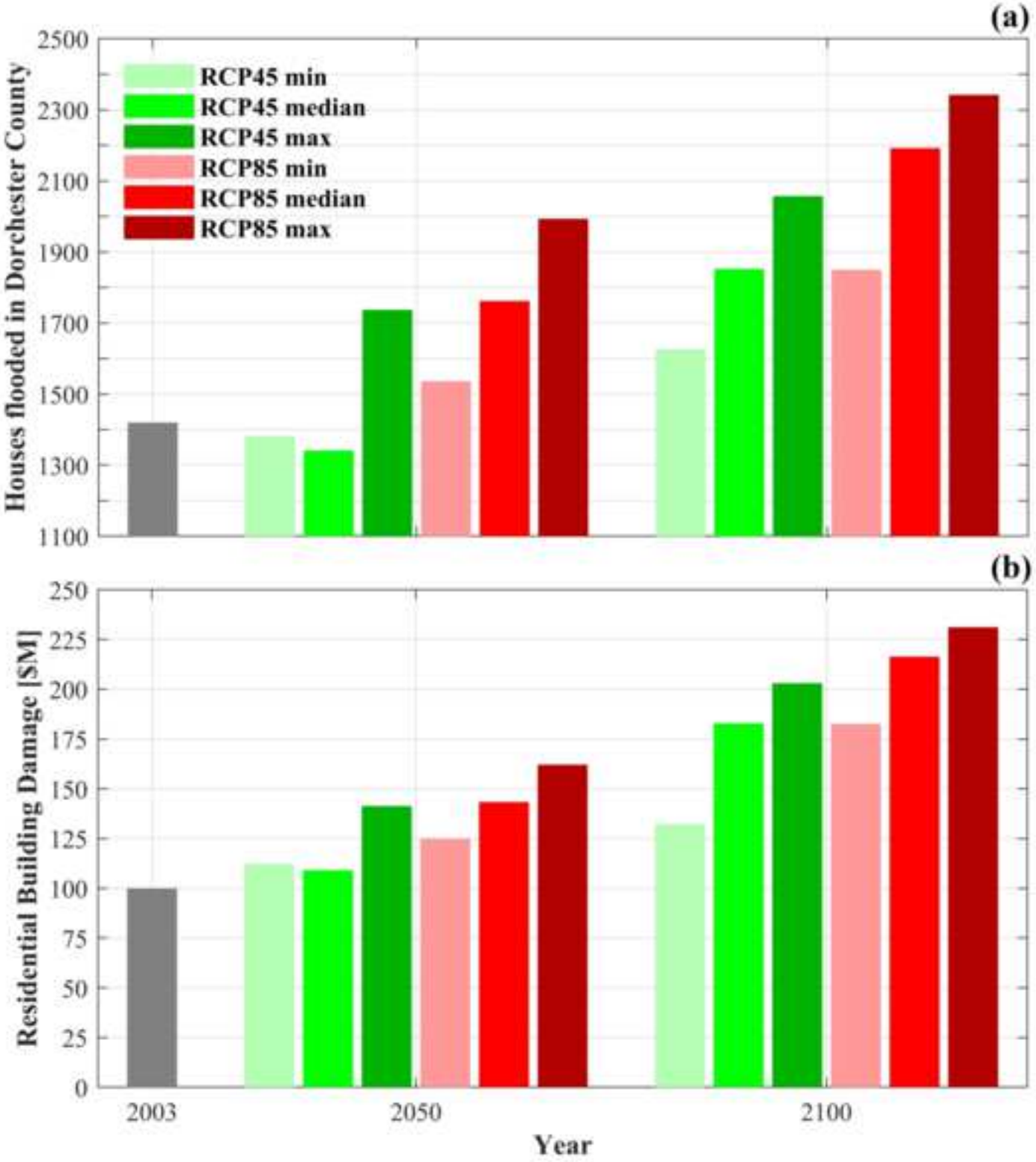

Figure 11

Click here to access/download;Figure;fig11.tif

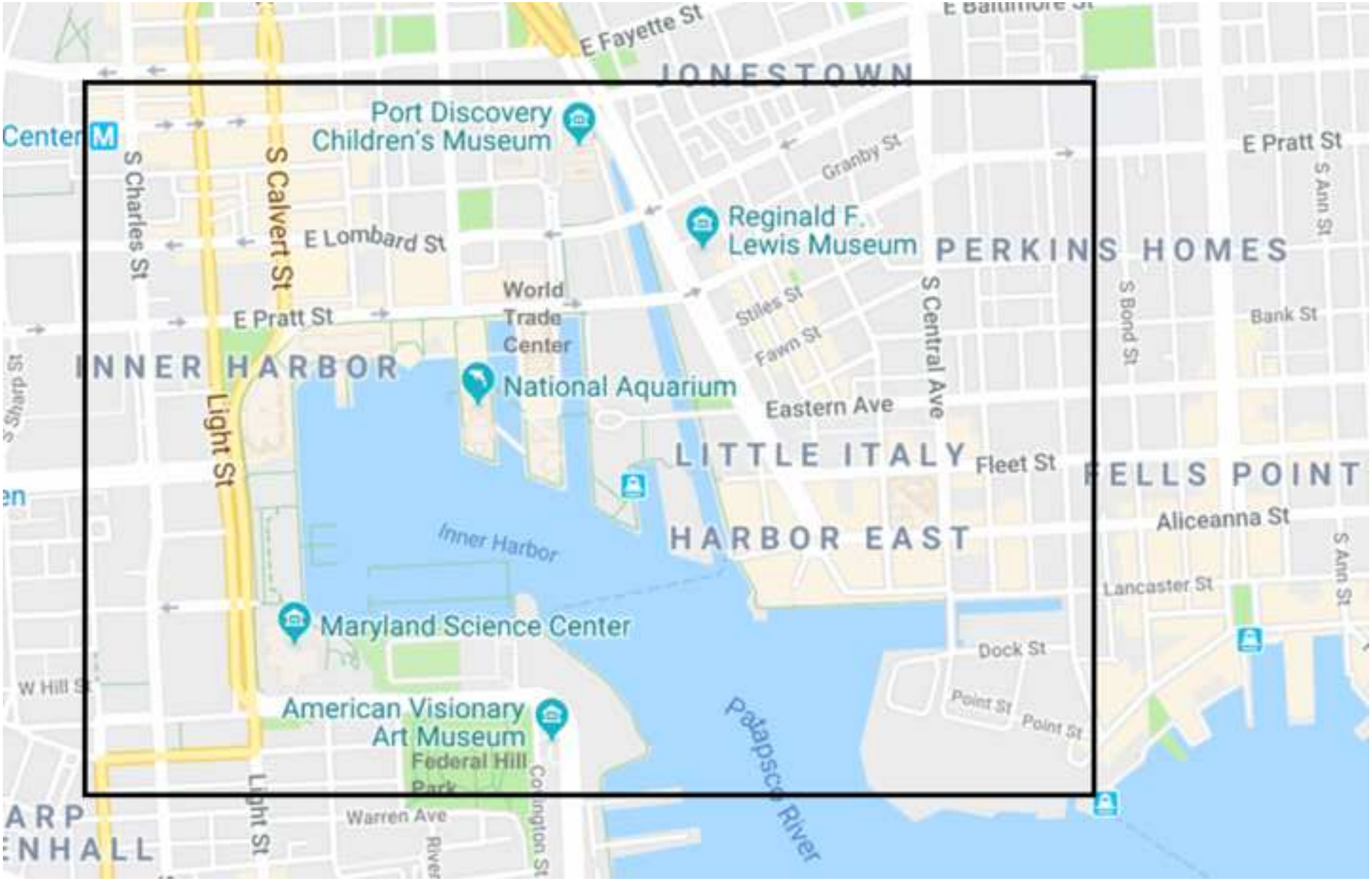

Figure 12

Click here to access/download;Figure;fig12.tif

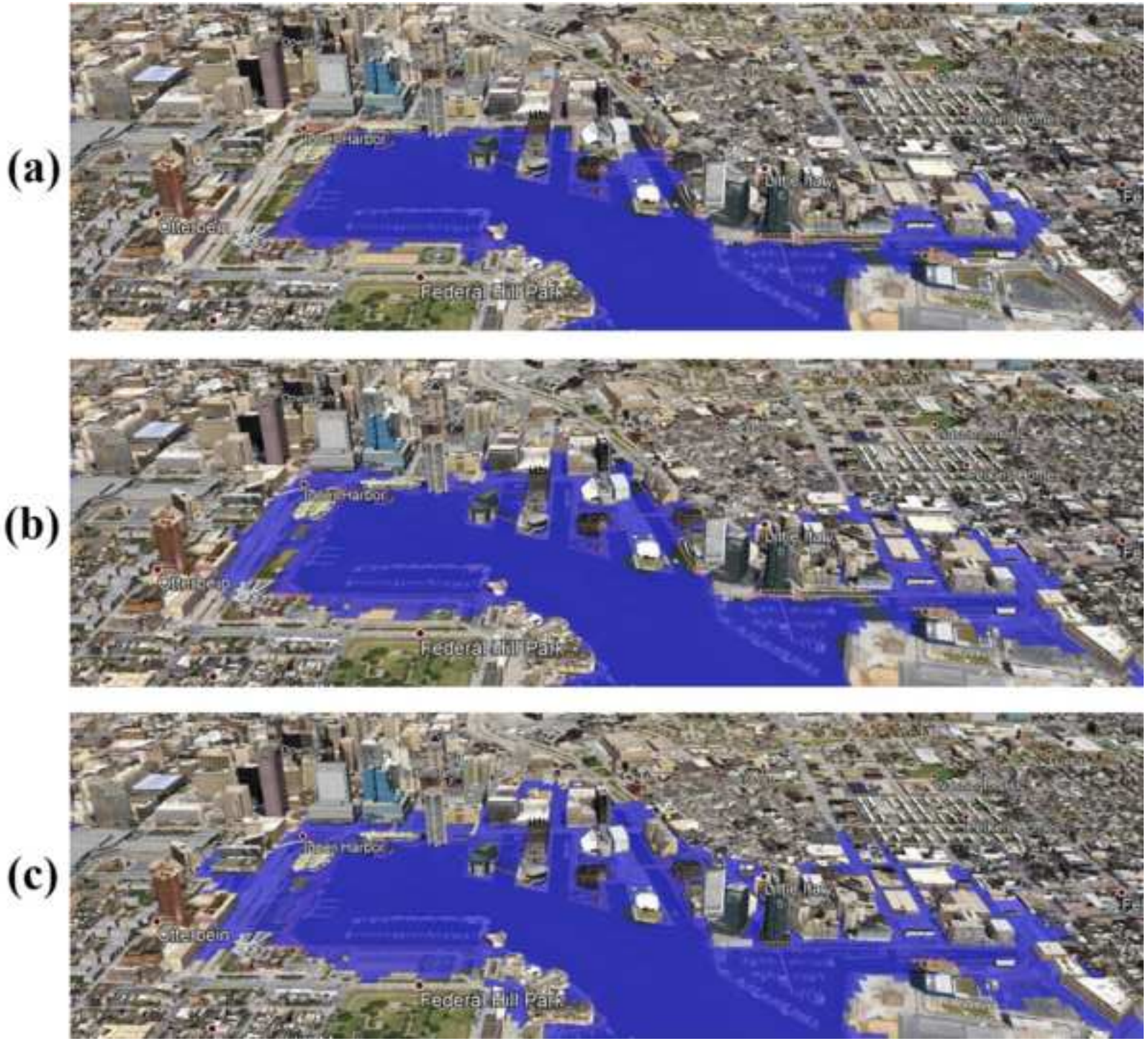

Figure 13

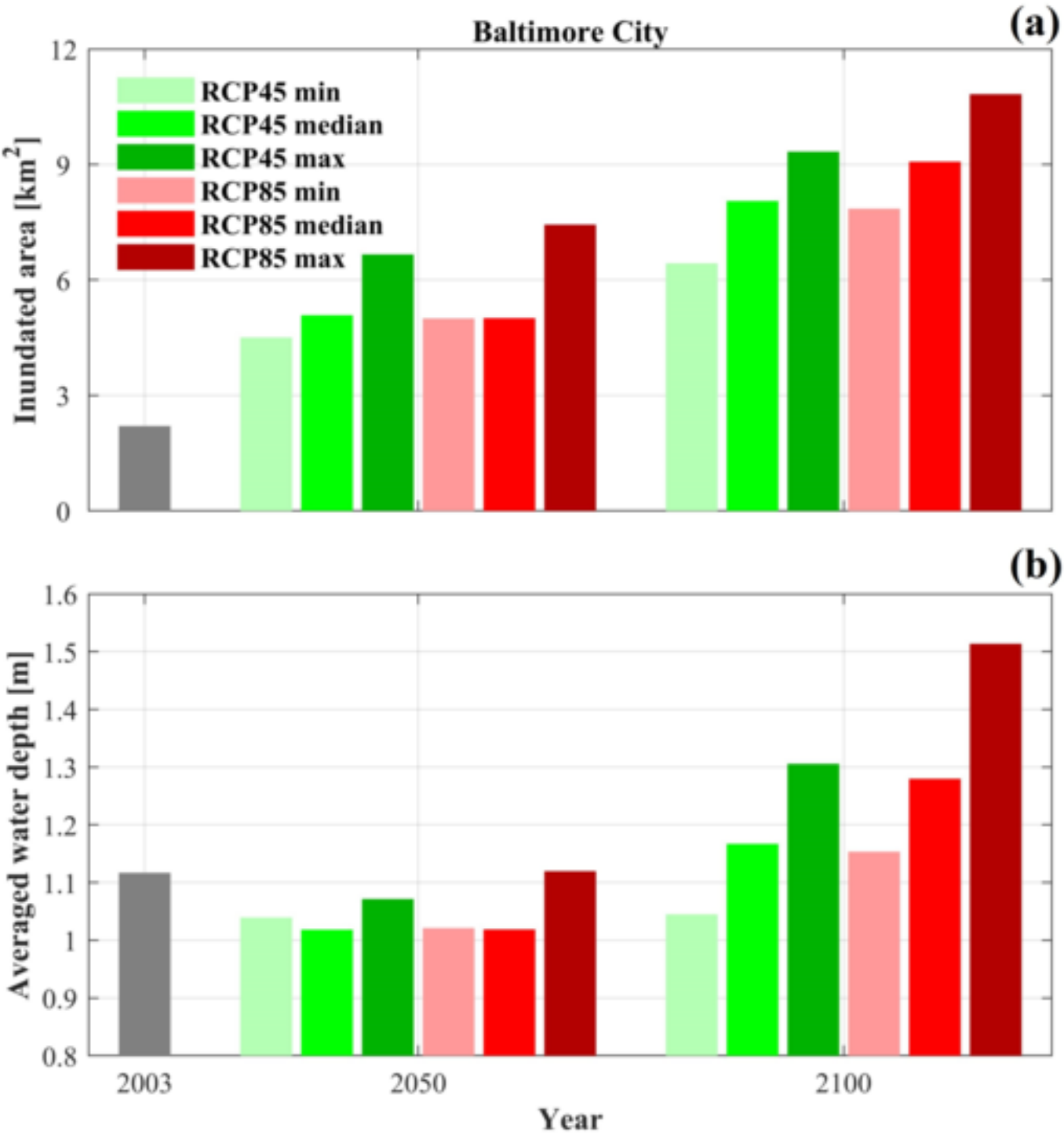

Figure 14

Click here to access/download;Figure;fig14.tif

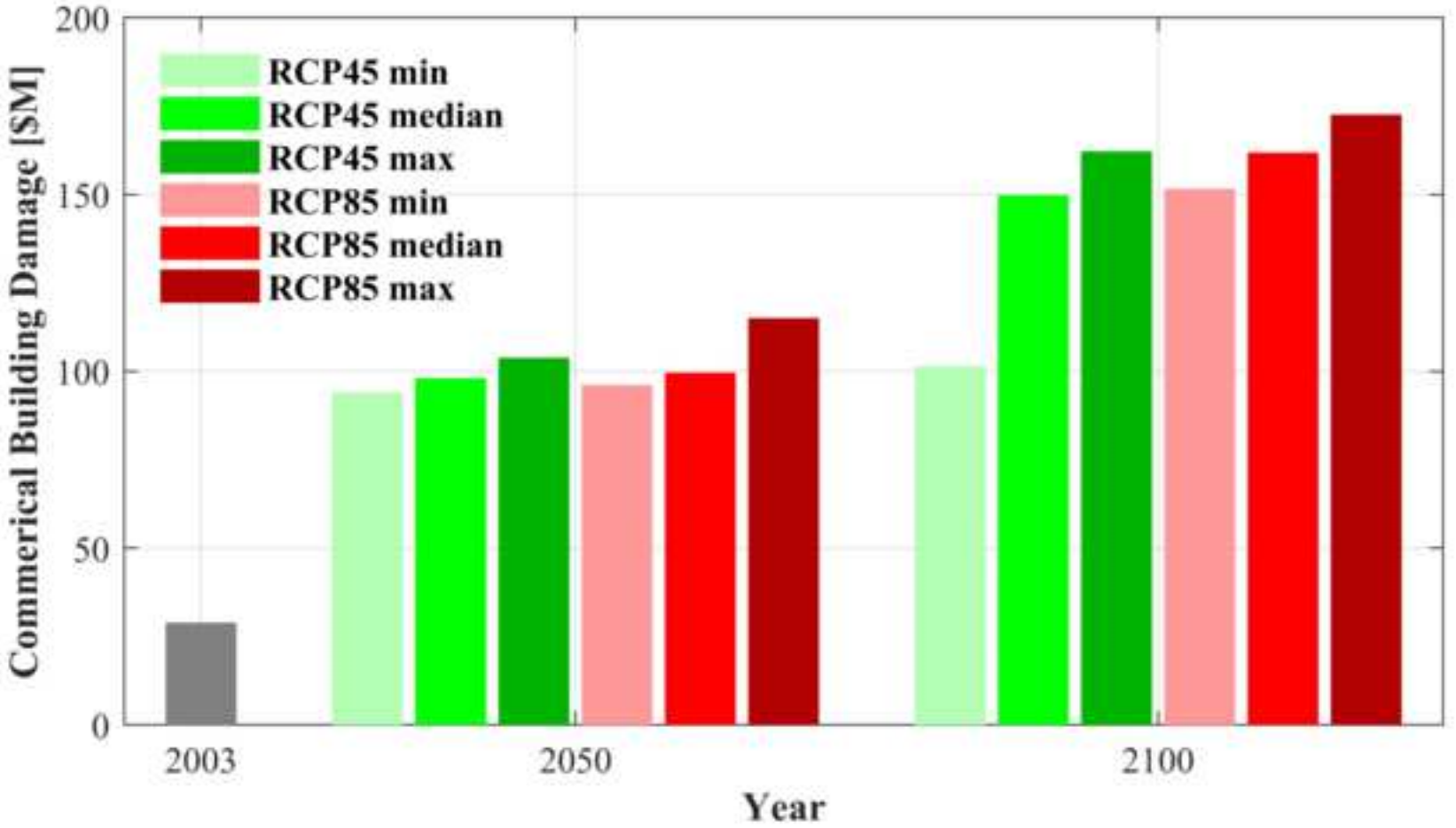

Table 1. Projected increases in sea surface temperature (SST) in the Atlantic ocean and relative sea level rise in Chesapeake Bay. The 'median', 'minimum', and 'maximum' scenarios are based on the median value and likely lower and upper bounds of projected global mean sea level rises in the IPCC AR5 report.

	RCP 4.5			**RCP 8.5**		
2050	median	minimum	maximum	median	minimum	maximum
SST increase in Tropical North Atlantic (ºC)	1.13	0.83	2.11	1.71	1.20	2.64
Global mean sea level rise	0.26	0.19	0.33	0.30	0.22	0.38
Regional ocean dynamics	0.09	0.07	0.10	0.09	0.07	0.1
Regional land subsidence	0.075	0.065	0.085	0.075	0.065	0.085
Relative sea level rise (m)	0.43	0.33	0.52	0.47	0.36	0.57
2100						
SST increase in Tropical North Atlantic (ºC)	1.48	0.98	2.54	2.94	2.30	4.24
Global mean sea level rise	0.53	0.36	0.71	0.74	0.52	0.98
Regional ocean dynamics	0.17	0.13	0.19	0.17	0.13	0.19
Regional land subsidence	0.15	0.13	0.17	0.15	0.13	0.17
Relative sea level rise (m)	0.85	0.62	1.07	1.06	0.78	1.34